EUROPEAN ORGANIZATION FOR NUCLEAR RESEARCH

Femtoscopic correlations of identical charged pions and kaons in pp collisions at $\sqrt{s}$ = 13 TeV with event-shape selection

ALICE Collaboration*

Abstract

Collective behavior has been observed in high-energy heavy-ion collisions for several decades. Collectivity is driven by the high particle multiplicities that are produced in these collisions. At the Large Hadron Collider (LHC), features of collectivity have also been seen in high-multiplicity proton–proton collisions that can attain particle multiplicities comparable to peripheral Pb–Pb collisions. One of the possible signatures of collective behavior is the decrease of femtoscopic radii extracted from pion and kaon pairs emitted from high-multiplicity collisions with increasing pair transverse momentum. This decrease can be described in terms of an approximate transverse mass scaling. In the present work, femtoscopic analyses are carried out by the ALICE collaboration on charged pion and kaon pairs produced in pp collisions at $\sqrt{s}$ = 13 TeV from the LHC to study possible collectivity in pp collisions. The event-shape analysis method based on transverse sphericity is used to select for spherical versus jet-like events, and the effects of this selection on the femtoscopic radii for both charged pion and kaon pairs are studied. This is the first time this selection method has been applied to charged kaon pairs. An approximate transverse-mass scaling of the radii is found in all multiplicity ranges studied when the difference in the Lorentz boost for pions and kaons is taken into account. This observation does not support the hypothesis of collective expansion of hot and dense matter that should only occur in high-multiplicity events. A possible alternate explanation of the present results is based on a scenario of common emission conditions for pions and kaons in pp collisions for the multiplicity ranges studied.

---

*See Appendix A for the list of collaboration members

arXiv:2310.07509v1 [nucl-ex] 11 Oct 2023

1 Introduction

The manifestation of collective effects in pp and p–A collisions with increasing multiplicity of charged particles is intensely discussed in the literature [1–3]. Surprisingly, these small colliding systems exhibit several signatures attributed to the formation of a strongly-interacting quark–gluon plasma in heavy-ion collisions, such as long-range ridge-like structures [4–6] and strangeness enhancement [7]. A full understanding of the mechanisms leading to collective effects observed in pp collisions at large multiplicity has not yet been achieved. For this reason, it is important to experimentally investigate the properties of small systems with the aim to discriminate between different theoretical models. Namely, the hydrodynamic models present the "heavy-ion view" of pp collisions e.g. Ref. [8], while string models are the "high-energy view" e.g. models including interactions between strings [9, 10].

The femtoscopy technique, which studies the final-state hadron–hadron interactions via their momentum correlations, is an effective tool for the extraction of the space–time characteristics of particle production processes, in particular the radii of the emitting source and the decoupling time. This method has already been employed in the past to study high-energy hadron–hadron [11, 12] and heavy-ion collisions [13, 14] using quantum statistical (QS) correlations and/or final-state interactions (FSI) of particles emitted with small relative momenta.

The characteristic feature of femtoscopy in heavy-ion collisions is the decrease of the source sizes for pairs of particles (with masses m and transverse momenta $\mathbf{p}_{T,1}$ and $\mathbf{p}_{T,2}$) with increasing pair transverse momentum $k_T = |\mathbf{p}_{T,1} + \mathbf{p}_{T,2}|/2$ or transverse mass $m_T = \sqrt{k_T^2 + m^2}$, see e.g. recent RHIC [15–17] and LHC [18, 19] results for pions. It was explained in Ref. [20] that femtoscopy measurements do not probe the whole volume in case of an expanding emitting source, but instead the region from which the particles with similar momenta are emitted, the so called "homogeneity volume". This region is smaller than the total volume occupied by the system and decreases with k_T (m_T). Several theoretical models based on the hydrodynamic approach successfully describe pion femtoscopy measurements e.g. Refs. [21–25]. It is expected that these models should describe the femtoscopy measurements for kaons and for heavier particles also, particularly the m_T and multiplicity dependencies of radii. In Ref. [26], it was shown that for the particular case of small transverse flow the hydrodynamics leads to the same m_T-behavior of the longitudinal radii (R_{long}) for pions and kaons. It means that the thermal freeze-out occurs simultaneously and that these two particle species are subject to the same velocity boost from collective flow. Modern calculations made within the 3+1D hydrodynamic model THERMINATOR-2 [23] at LHC energies demonstrate the approximate m_T scaling of the three-dimensional radii for pions, kaons and protons [25] when the radii versus m_T fall with some degree of accuracy on one curve. The authors of Ref. [25] also investigated one-dimensional radii (R_{inv}) in pair reference frame (PRF) for the case of lack of available experimental data. They have verified that the violation of this scaling in the case when the three-dimensional scaling is presented in the model has a trivial kinematic origin. It is possible to take it into account and restore the m_T scaling for R_{inv} for pions, kaons, and protons. The calculations performed within the Hydro-Kinetic Model, including not only a hydrodynamic phase but also the hadronic rescattering stage, predicted violation of this scaling between pions and kaons at LHC energies [27, 28], mainly due to the rescatterings in the hadronic phase. ALICE results for Pb–Pb collisions at $\sqrt{s_{NN}} = 2.76$ TeV [29] have shown that the m_T scaling expected by pure hydrodynamical scenarios is broken. The comparison of these two different evolution scenario demonstrate the importance of the m_T scaling study.

At the LHC, the femtoscopic sizes range for various colliding systems from 2–7 fm for Pb–Pb to 1–2 fm for pp and p–Pb collisions, which opens a possible access to different energy densities of the system created during such collisions and probably helps understand the conditions required for the QGP formation. The multiplicity and m_T dependencies were studied for pions and kaons by ALICE for Pb–Pb collisions e.g. Refs. [19, 29] and for pp and p–Pb collisions e.g. Refs. [30, 30–35]. In pp collisions, it was observed for both types of pairs that for higher charged-particle multiplicity ranges

the measured size of the source decreased with increasing m_T, similarly to the trend seen in heavy-ion collisions. Instead, at low charged-particle multiplicities, the measured source radii increased with increasing m_T [30, 30, 32, 33]. Unfortunately, there are almost no theoretical models for pp collisions which include the space–time coordinates and can be used to describe femtoscopic observables. Attempts to describe the behavior of femtoscopic radii in pp collisions at the LHC from the hydrodynamic point of view were performed in e.g. Refs. [36, 37], from the view of the uncertainty principle in Ref. [38], from the view of the string models in Ref. [39] using LUND hadronization scheme which automatically introduces the space–momentum correlations similar to the correlations in hydrodynamic models, where they arise due to transverse collective flow.

The study of femtoscopic correlations in pp collisions is more challenging than in A–A collisions due to the strong non-femtoscopic contributions, i.e. correlations due to multi-body resonance decays, mini-jets, and energy-momentum conservation. Typically, a baseline distribution function is constructed to remove these non-femtoscopic effects, after which the hadron–hadron correlations due to pure QS and FSI can be studied. There are various methods to exclude them: (1) the so called "double ratio" technique, dividing the experimental correlation function by the baseline extracted from Monte Carlo simulations [30]; (2) the "cluster subtraction" technique, using the opposite-sign pair (e.g. $\pi^+\pi^-$) distributions as a baseline [40]; (3) a "hybrid method" between (1) and (2), as described in Ref. [40, 41]) and (4) the three-particle cumulant method [42], which significantly suppresses the mini-jet related contributions and can be used as an alternative to the study of two-particle correlations.

A method to suppress, in particular, mini-jet contributions in two-particle correlation functions was suggested in Ref. [43] and it is based on applying event-shape selections. It was shown that it is possible to differentiate between jet-like and spherical event topologies using a global characteristic of the event such the transverse sphericity [44, 45] and the transverse spherocity [46, 47]. It was observed for the first time in Ref. [43] that the pion radii for jet-like events are smaller than the source radii for spherical events. In jet-like events, the radii dependence on multiplicity is such that they increase with increasing k_T in the lowest multiplicity interval and decrease with k_T for the highest multiplicities. There are no multiplicity dependence for these events. The radii for spherical events show an increase in system size with increasing multiplicity. They do not show any visible trend with k_T, which differs from the results of sphericity-integrated (minimum-bias) pion and kaon analyses in Refs. [30, 33], where the obtained radii decrease with increasing k_T. This different behavior suggests [43] that the lower part of the transverse sphericity spectrum contributes to the observed slope in minimum bias (MB) pp collisions.

In this work, the femtoscopic correlations of identical charged pions and kaons are investigated in pp collisions at $\sqrt{s} = 13$ TeV. The purpose of this analysis is to study the transverse-momentum and multiplicity dependence of pion and kaon femtoscopic radii separately for jet-like and spherical events. The influence of the sphericity selections on the kaon femtoscopic radii is studied for the first time.

The article is organized as follows. Section 2 briefly describes the ALICE experimental setup. Section 3 presents the event selection criteria. Section 4 introduces the definition of sphericity, discusses the analysis methods to extract the femtoscopic correlation function for pion and kaon pairs and the estimation of the systematic uncertainties. The extracted femtoscopic parameters are shown and discussed in Section 5. The results are summarized in Section 6.

2   Experimental setup

A detailed description of the ALICE detector and its performance can be found in Refs. [48, 49]. In the present analysis, the information from the Inner Tracking System (ITS) [50], the Time Projection Chamber (TPC) [51], the Time-Of-Flight (TOF) [52], and the V0 [53] detectors are used.

The V0 detector is used for triggering on collision events. It is composed of two small-angle scintillator

3

arrays, located at 340 cm and 90 cm from the nominal interaction point along the beam line and covering $2.8 < \eta < 5.1$ (V0A) and $-3.7 < \eta < -1.7$ (V0C), respectively. The events are selected with the MB trigger, which requires simultaneous signals in both parts of the V0 detector in coincidence with two beam bunches crossing in the ALICE interaction region. The rejection of pile-up events is performed by using the vertexing capabilities of the Silicon Pixel Detector (SPD) [49], which forms the two innermost layers of the ITS. Events with multiple vertices identified with the SPD (in-bunch pile-up) are removed from the analysis. Pile-up events from different bunch crossings are rejected by requiring the tracks to have hits in the SPD. The remaining leftover pile-up is negligible in the present analysis.

Charged particles are reconstructed with the central barrel ITS and TPC detectors placed inside a solenoidal magnet providing a uniform 0.5 T field parallel to the beam direction. The primary vertex is reconstructed using the ITS. This detector is a silicon tracker with six layers of silicon sensors covering the pseudorapidity range $|\eta| < 0.9$ [50]. The TPC is the main tracking detector in ALICE, which measures the ionization energy loss of particles. The chamber is divided into two halves by a central electrode. The end caps on either side are composed of 18 sectors (covering the full azimuthal angle) with 159 pad rows placed radially in each sector. The TPC covers an acceptance of $|\eta| < 0.9$ for tracks which reach the outer radius of the detector.

Particle identification (PID) for reconstructed tracks is carried out using the TPC together with the TOF [52] detectors. The TOF is a cylindrical detector consisting of 18 azimuthal sectors divided into five modules along the beam axis with active element multi-gap resistive plate chambers. Pions and kaons were identified using the TPC and TOF detectors. The deviation of the specific energy loss (dE/dx) measured in the TPC from the one calculated using the Bethe–Bloch parametrization was required to be within a certain number of standard deviations ($n_{\sigma_{TPC}}$). A similar $n_{\sigma_{TOF}}$ method was applied for the particle identification in the TOF. The deviation is computed between the measured time of flight and the one calculated for a given particle path length, momentum, and mass.

3   Data selection

The data samples used in this work were recorded by ALICE in 2016–2018 during the LHC Run 2 period at $\sqrt{s} = 13$ TeV. After application of all selection criteria, about 10^9 minimum bias events were analyzed.

Events were accepted if they had the collision vertex position measured along the beam line within ± 10 cm from the nominal interaction point. The charged particle tracks were required to be reconstructed with the ITS and TPC detectors with a χ^2 per number of degrees of freedom (χ^2/NDF) smaller than 4.0 and each track segment was reconstructed from at least 70 out of the 159 possible space points. The distance of closest approach (DCA) to the primary vertex was required to be smaller than 0.3 cm in both the transverse plane and the longitudinal direction.

Femtoscopic correlation functions of identical particles are sensitive to two-track reconstruction effects because the particles of interest have close momenta and close trajectories. Two kinds of two-track effects, splitting and merging, were studied. The splitting of the tracks means that one track is reconstructed as two. The track merging means that two different tracks are reconstructed as one. To remove these effects, the distance between the tracks of two particles was calculated at up to nine points throughout the TPC volume (every 20 cm from 85 cm to 245 cm in radial direction) and then averaged. It was required that the particles for each pair had an average TPC separation of at least 3 cm.

Pions and kaons were selected in the pseudorapidity $|\eta| < 0.8$ range. For pions, the transverse momentum $0.15 < p_T < 4.0$ GeV/c range was used. The pion selection criteria are presented in Table 1. The pion purity is about 99% for track momenta $p < 2.0$ GeV/c, while, for the $2 < p_T < 4$ GeV/c interval, it decreases to 80% due to an increasing contamination from kaons.

The selection criteria for the kaons are reported in Table 2. In order to avoid strong contamination from

Table 1: Charged pion selection criteria.

Selection criterium	Value
p_T	$0.15 < p_T < 4.0$ GeV/c
$|\eta|$	< 0.8
DCA$_{transverse}$	< 0.3 cm
DCA$_{longitudinal}$	< 0.3 cm
$n_{\sigma_{TPC}}$	< 3 (for $p < 0.5$ GeV/c)
$\sqrt{n_{\sigma_{TPC}^2} + n_{\sigma_{TOF}}^2}$	< 3 (for $0.5 < p < 4.0$ GeV/c)
Number of track points in TPC	≥ 70

Table 2: Charged kaon selection criteria.

Selection criterium	Value
p_T	$0.15 < p_T < 1.5$ GeV/c
$|\eta|$	< 0.8
DCA$_{transverse}$	< 0.3 cm
DCA$_{longitudinal}$	< 0.3 cm
$n_{\sigma_{TPC}}$	< 2 (for $0.15 < p < 0.4$ GeV/c)
	< 1 (for $0.4 < p < 0.45$ GeV/c)
	< 2 (for $0.45 < p < 1.5$ GeV/c)
$n_{\sigma_{TOF}}$	< 2 (for $0.5 < p < 0.8$ GeV/c)
	< 1.5 (for $0.8 < p < 1.0$ GeV/c)
	< 1.0 (for $1.0 < p < 1.5$ GeV/c)
Number of track points in TPC	≥ 70

pions, narrower momentum ranges were used for kaons, namely $0.15 < p_T < 1.5$ GeV/c. The dominant contamination for charged kaons is from e$^{\pm}$ in the particle momentum range $0.4 < p < 0.5$ GeV/c resulting in a kaon purity of approximately 90%. Outside this range, the kaon purity is about 99%.

4 Analysis technique

Pions and kaons were selected in the same raw charged-particle multiplicity intervals N_{trk} of (1–18), (19–30), and (> 30) in order to compare the obtained results in the same multiplicity conditions. The sphericity calculations (see Section 4.1) require at least three tracks with $p_T > 0.5$ GeV/c. Therefore, the lowest multiplicity interval is (1–18) if the sphericity calculation is not performed, while it is (3–18) when the sphericity is calculated. From now on, the lowest multiplicity interval will be denoted as (1–18) for both cases. The multiplicity for primary charged tracks [54] was estimated using the combined reference multiplicity estimator (SPD tracklets and tracks reconstructed in the ITS and the TPC) in the $|\eta| < 0.8$ range. The SPD tracklets are track segments built by associating pairs of hits in the two SPD layers. For each raw multiplicity interval, the average charged-particle pseudorapidity density $\langle dN_{ch}/d\eta \rangle$ was obtained by converting the measured event multiplicities using Monte Carlo simulations with the PYTHIA 8.2 event generator [55] (with the Monash tune [56]) and the GEANT3 package [57] for the transport of the generated particles through the ALICE detector. The intervals and their corresponding $\langle dN_{ch}/d\eta \rangle$, for both cases with and without sphericity event selections (S_T, defined in next section), are shown in Table 3. The systematic uncertainties for these densities were evaluated as the difference between their magnitudes when taking into account or not the detector efficiency correction using the Monte Carlo simulation mentioned above. The estimated value for these uncertainties is about 5 %.

Table 3: Raw charged-particle multiplicity (N_{trk}) intervals and corresponding average $\langle \text{d}N_{\text{ch}}/\text{d}\eta \rangle$ calculated from corrected multiplicity distributions in the $|\eta| < 0.8$ range. The values are quoted with their systematic uncertainties, the statistical uncertainties are negligible.

N_{trk}	$\langle \text{d}N_{\text{ch}}/\text{d}\eta \rangle_{S_{\text{T}}>0.7}$	$\langle \text{d}N_{\text{ch}}/\text{d}\eta \rangle_{S_{\text{T}}<0.3}$	$\langle \text{d}N_{\text{ch}}/\text{d}\eta \rangle$
3(1)–18	7.8 ± 0.4	6.2 ± 0.3	5.1 ± 0.2
19–30	15.0 ± 0.7	13.5 ± 0.6	14.3 ± 0.7
> 30	25.4 ± 1.0	21.8 ± 0.9	24.7 ± 0.1

4.1 Transverse sphericity

In collider experiments, the study of the shape of the emitting source is often performed in the transverse x–y plane in order to avoid distortions related to the Lorentz boost in the beam direction along the z axis [45]. Following this principle, the transverse sphericity (S_{T}) was used to study event characteristics in pp collisions at the LHC by the ALICE Collaboration [58]. The transverse sphericity is defined as

$$S_{\text{T}} = \frac{2\min(\lambda_1, \lambda_2)}{\lambda_1 + \lambda_2}, \tag{1}$$

where λ_1 and λ_2 are the eigenvalues of the matrix of transverse particle momenta

$$S_{\text{T}} = \frac{1}{\sum_i p_{\text{T}}^i} \sum_i \frac{1}{p_{\text{T}}^i} \begin{pmatrix} (p_{\text{x}}^i)^2 & p_{\text{x}}^i p_{\text{y}}^i \\ p_{\text{x}}^i p_{\text{y}}^i & (p_{\text{y}}^i)^2 \end{pmatrix}, \tag{2}$$

with p_{x}^i and p_{y}^i being the components of the transverse momentum for i-th particle $\vec{p}_{\text{T}}^i$. The transverse sphericity takes values in the (0–1) range. By definition of sphericity, in case of $S_{\text{T}} \to 0$, the emitting source is a strongly elongated ellipse, while $S_{\text{T}} \to 1$ corresponds to a nearly isotropic source in momentum or coordinate space. To ensure good resolution of the transverse sphericity calculation, only events with more than two primary tracks in $|\eta| < 0.8$ and $p_{\text{T}} > 0.5$ GeV/c were selected [44]. Following Ref. [43], $S_{\text{T}} > 0.7$ was used in this analysis to select spherical events. It is expected that for these events, the multiple soft particle production processes dominates. For jet-like events with $S_{\text{T}} < 0.3$, hard processes such as jets and mini-jets become dominant.

Figure 1 shows the experimental probability of having events with different transverse sphericity for the given raw multiplicity intervals: (1–18), (19–30), and (> 30). Sphericity is correlated with multiplicity, so the number of events with small S_{T} values is higher in the lowest multiplicity interval, while the larger multiplicity intervals contain more events with large sphericity values.

The difference between spherical events, jet-like events, and events without sphericity selection can be clearly seen in Fig. 2, which presents the experimental and Monte Carlo distributions of the azimuthal angle difference $\Delta\varphi$ between the trigger and the associated particles, where the trigger particle is the particle with the largest p_{T} in the event, $p_{\text{T}}^{\text{trig}} > 0.5$ GeV/c, $p_{\text{T}}^{\text{assoc}} < p_{\text{T}}^{\text{trig}}$. All distributions are normalized by the number of associated particles: $N_{\text{assoc}}(S_{\text{T}}(0,1)) = N_{\text{assoc}}(S_{\text{T}} < 0.3) + N_{\text{assoc}}(S_{\text{T}} > 0.7) + N_{\text{assoc}}(S_{\text{T}}(0.3, 0.7))$.

The Monte Carlo simulations with PYTHIA 8 as event generator and GEANT 3 for the simulation of the detector and the propagation of particles through the detector material, describe the $\Delta\varphi$ distributions reasonably well for all sphericity selections. The jet-like events demonstrate a strong anisotropic structure. The peak at $\Delta\varphi \sim 0$ corresponds to correlations within the jet determined by the trigger particle. The peak at $\Delta\varphi \to \pi$ corresponds to the correlation of the particle associated with the jet moving in the opposite direction. Both peaks are absent for the sphericity selection $S_{\text{T}} > 0.7$. The $\Delta\varphi$ distribution shows some specific features with respect to the distribution without sphericity selection, which are reasonably well described by PYTHIA 8. The spherical events are much more isotropic than the jet-like ones, and the jet structures are suppressed.
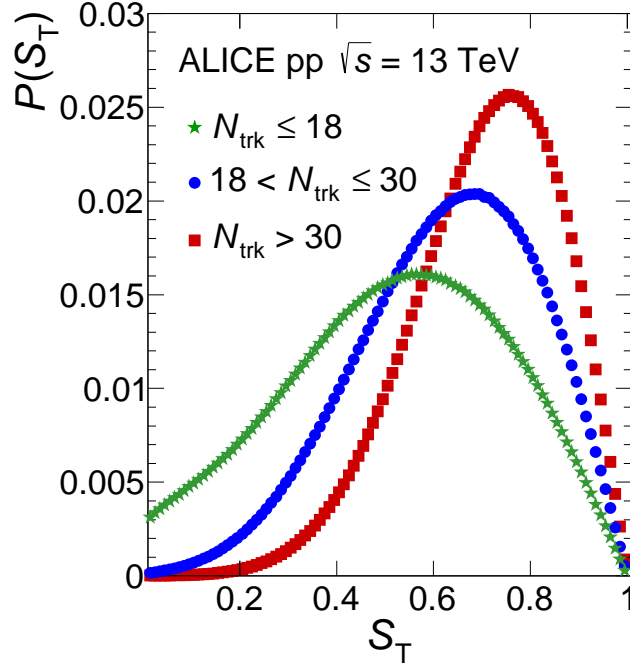
Figure 1: The experimental probability P of having events of different transverse sphericity S_T in the given raw multiplicity N_{trk} intervals: (1–18), (19–30), and (> 30). There are no corrections applied for the efficiency of the sphericity selection. Only statistical uncertainties are shown and are smaller than the marker size.

4.2 Correlation functions

The particle source created in hadronic or nuclear collisions is usually investigated using momentum correlations of two or more emitted particles. This analysis studies two-particle correlations. The observable of interest is the correlation function (CF) defined as

$$C(\mathbf{p}_1, \mathbf{p}_2) = A(\mathbf{p}_1, \mathbf{p}_2)/B(\mathbf{p}_1, \mathbf{p}_2), \tag{3}$$

where $A(\mathbf{p}_1, \mathbf{p}_2)$ is the two-particle momentum distribution in the given event, and $B(\mathbf{p}_1, \mathbf{p}_2)$ is a reference distribution [59]. The former includes information on the source as well as on the FSI of the emitted hadrons and/or QS effects. The latter is constructed by mixing particles emitted in two different collisions to avoid any influence of pair correlation. In the present work, the reference distribution is constructed by mixing ten events with similar multiplicity and of close sphericities. It is also required that events in a mixed event pool have their vertex positions within 2 cm from each other along the beam direction.

Due to the experimental limitation in the number of pairs, the CF is commonly defined in terms of a single kinematic variable instead of using the particle momentum vectors (see Eq. (3)). In the following, the Lorentz-invariant $q_{inv} = \sqrt{\mathbf{q}^2 - q_0^2}$ is used, where $\mathbf{q} = \mathbf{p}_1 - \mathbf{p}_2$ is the pair momentum difference and $q_0 = E_1 - E_2$ is the energy component difference.

The measured correlation functions are corrected using the so called double-ratio technique for the MC simulated ones $C_{MC}(q_{inv})$. This procedure assumes that the signal and the background are factorized. The corrected correlation function can be written as

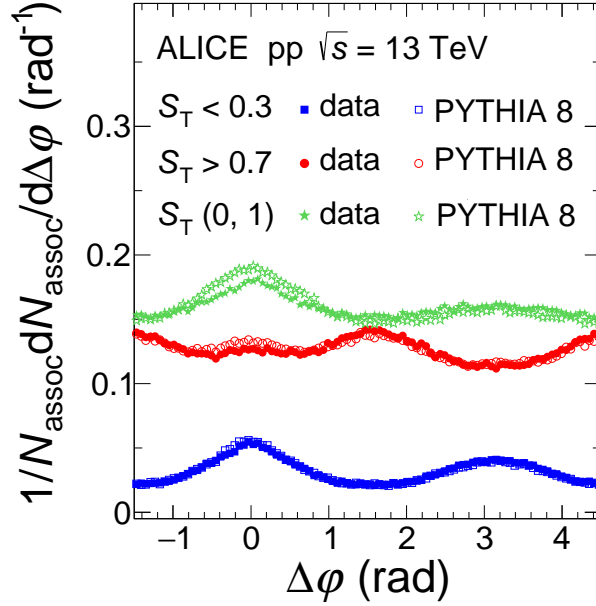$$C_{corr}(q_{inv}) = \frac{C_{data}(q_{inv})}{C_{MC}(q_{inv})}. \tag{4}$$

7

Figure 2: The pion raw experimental distribution of the azimuthal angle difference $\Delta\varphi$ between the trigger and the associated particles for $S_{\mathrm{T}} > 0.7$ (red circles), $S_{\mathrm{T}} < 0.3$ (blue squares) and S_{T} (0,1) (green stars) compared with MC PYTHIA 8 calculations shown with the corresponding open markers. The calculations include particle transport through the ALICE detector using the GEANT 3 transport package. The statistical uncertainties are smaller than the marker size.

Generally, the CF includes several effects, such as femtoscopic effects (QS+Coulomb in the case of $\pi^{\pm}\pi^{\pm}$ and $\mathrm{K}^{\pm}\mathrm{K}^{\pm}$ correlations), mini-jet contributions at low q_{inv}, and long-range correlations due to energy–momentum conservation at high q_{inv}. The latter are present in the same-event pair relative-momentum distribution and absent in the mixed-event distribution determining the CFs. If spherical events are selected with $S_{\mathrm{T}} > 0.7$, contributions of mini-jets are strongly suppressed. However, there is still influence of long-range correlations due to the conservation laws. Therefore, to correct the experimental CFs for these long-range effects in spherical events, a MC model which correctly describes the shape of the experimental CFs at large q_{inv} are used. The experimental CFs can be divided by the MC ones (Eq. (4)), and the resulting CFs are considered to contain only femtoscopic effects, which can be fitted with a function including QS and Coulomb interaction. For pp collisions at $\sqrt{s} = 13$ TeV, the PYTHIA 8 [55] MC model gives the best description of the experimental function outside the low q_{inv} region. For jet-like ($S_{\mathrm{T}} < 0.3$) events, there is a large contribution of mini-jets at low q_{inv} in addition to the long-range correlations at high pair relative momentum. They can also be corrected using PYTHIA 8 calculations in order to consider femtoscopic correlations only.

The analysis was performed separately for positively and negatively charged pions and kaons at two magnetic field polarities, after which the two-particle correlations were combined using their statistical uncertainties as weights.

The analysis for pions and kaons was performed in the same three multiplicity intervals. For pions, five pair transverse momentum k_{T} intervals were used: (0.15–0.3), (0.3–0.5), (0.5–0.7), (0.7–0.9), and (0.9–1.2) GeV/c. The analysis for kaons was performed in two k_{T} intervals: (0.15–0.5), (0.5–1.2) GeV/c.

8

4.2.1 Pion correlation functions

Figure 3 shows the pion experimental CF (green solid circles) for events with $S_T > 0.7$ in pp collisions at $\sqrt{s} = 13$ TeV. The PYTHIA 8 (Monash) model calculations including the ALICE detector response were used to describe non-femtoscopic effects and are also shown in the figure (blue crosses). All distributions are normalized to unity in the $0.7 < q_{inv} < 0.8$ GeV/c range, which is well outside the QS and Coulomb FSI region ($q_{inv} \lesssim 0.4$ GeV/c) and before the noticeable large q_{inv} slope associated with energy and momentum conservation. The CFs shown in Fig. 3 are flat for the low multiplicity intervals in the region $0.5 < q_{inv} < 1.0$ GeV/c. For the two highest k_T intervals, some slope of baseline appears. At $q_{inv} > 1.0$ GeV/c, the aforementioned kinematic effects are present especially for the lowest multiplicity intervals.

The CFs decrease at $q_{inv} \to 0$ for the PYTHIA 8 calculations for the lowest multiplicity interval ($N_{trk} \leq 18$) in the (0.5–0.7) GeV/c, (0.7–0.9) GeV/c and (0.9–1.2) GeV/c k_T intervals. The occurrence of such minima is related to the three tracks requirement, necessary for the transverse sphericity calculation [44]. Indeed, the number of available events with three tracks with $p_T > 0.5$ GeV/c decreases at small q_{inv}.
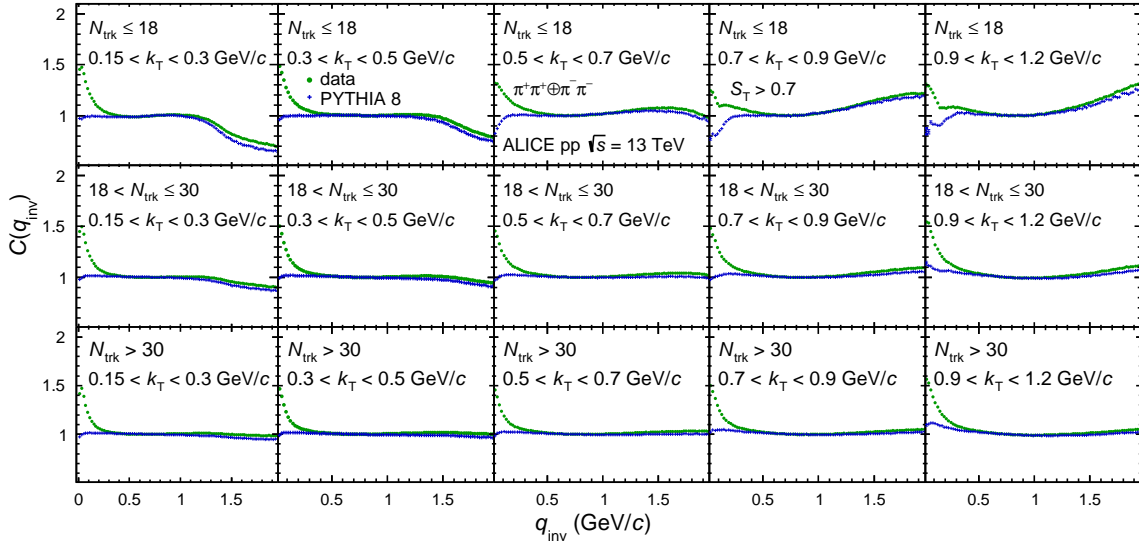
Figure 3: The $\pi^{\pm}\pi^{\pm}$ experimental correlation functions (green solid circles) as function of the invariant pair relative momentum q_{inv} in pp collisions at $\sqrt{s} = 13$ TeV for the raw multiplicity N_{trk} intervals of (1–18), (19–30), and (> 30) in the (0.15–0.3) GeV/c, (0.3–0.5) GeV/c, (0.5–0.7) GeV/c, (0.7–0.9) GeV/c and (0.9–1.2) GeV/c k_T intervals. A sphericity selection of $S_T > 0.7$ is applied. The data are compared with PYTHIA 8 calculations, shown by blue crosses. The error bars represent the statistical uncertainties, while the systematic uncertainties are negligible.

Figure 4 illustrates the pion experimental correlation function in pp collisions at $\sqrt{s} = 13$ TeV compared with PYTHIA 8 model calculations for events with $S_T < 0.3$. The CFs for jet-like events shown in this figure exhibit a pronounced slope over the full q_{inv} range indicating the presence of non-femtoscopic effects. These effects are especially pronounced for $k_T > 0.5$ GeV/c. As can be seen from the figure, the PYTHIA 8 model calculations describe reasonably well the pion experimental data for jet-like events at large q_{inv} values.

4.2.2 Kaon correlation functions

Figure 5 shows the kaon experimental CF (green solid circles) for events with $S_T > 0.7$ and the corresponding PYTHIA 8 calculations (blue crosses) in pp collisions at $\sqrt{s} = 13$ TeV.
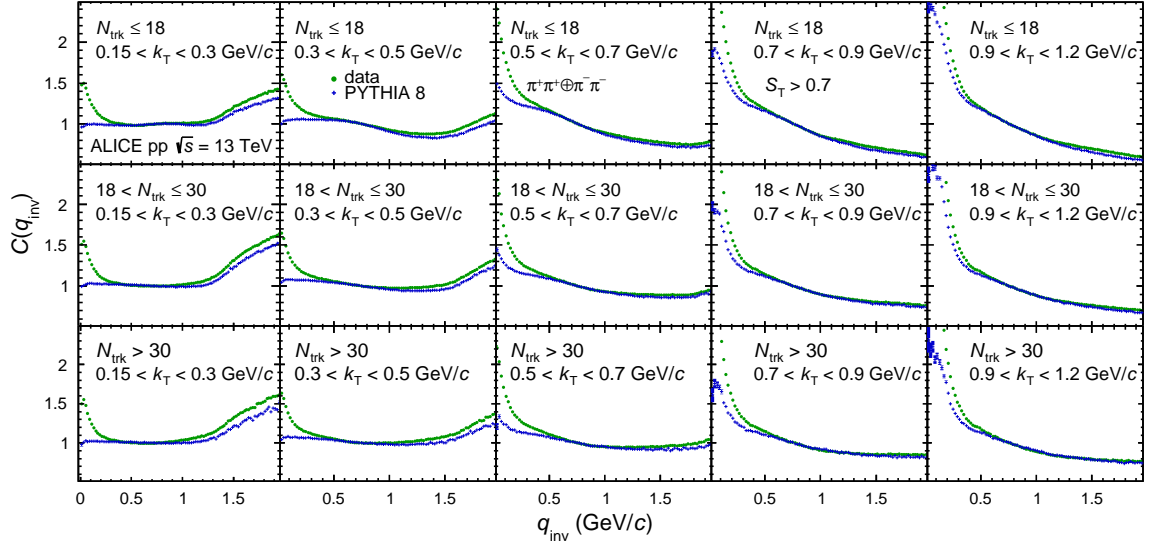
Figure 4: The $\pi^\pm\pi^\pm$ experimental correlation functions (green solid circles) as function of the invariant pair relative momentum q_{inv} in pp collisions at $\sqrt{s} = 13$ TeV for the raw multiplicity N_{trk} intervals of (1–18), (19–30), and (> 30) in the (0.15–0.3) GeV/c, (0.3–0.5) GeV/c, (0.5–0.7) GeV/c, (0.7–0.9) GeV/c and (0.9–1.2) GeV/c k_{T} intervals. A sphericity selection of $S_{\mathrm{T}} < 0.3$ is applied. The data are compared with PYTHIA 8 calculations shown by blue crosses. The error bars represent the statistical uncertainties, while the systematic uncertainties are negligible.

The strength of the charged kaon correlations, represented by the magnitude of $C(q_{\mathrm{inv}})$ for $q_{\mathrm{inv}} \to 0$, is smaller than observed for the pions and decrease with k_{T}. The CFs for spherical events are flat at $q_{\mathrm{inv}} > 0.5$ GeV/c both for the data and the MC calculations. The non-femtoscopic background contributions obtained using PYTHIA 8 were fitted with a second-order polynomial, which then was used for the correction of the experimental CFs for non-femtoscopic effects. The fit allows reducing the impact of statistical fluctuations on the extracted femtoscopic parameters.

Figure 6 presents the kaon experimental correlation function for events with $S_{\mathrm{T}} < 0.3$ in pp collisions at $\sqrt{s} = 13$ TeV, for the raw multiplicity intervals N_{trk} of (1–18), (19–30), and (> 30) in the (0.15–0.5) GeV/c and (0.5–1.2) GeV/c k_{T} intervals. Similarly to the pion CFs for jet-like events (see Fig. 4), the kaon jet-like CFs shown in Fig. 6 exhibit a pronounced slope at low q_{inv} indicating the presence of non-femtoscopic effects. Such background is especially pronounced for $k_{\mathrm{T}} > 0.5$ GeV/c. As can be seen in the figure, the estimate of the femtoscopic signal with respect to the background effects in the highest $N_{\mathrm{trk}} > 30$ multiplicity interval is not possible since the correlation functions coincide with PYTHIA 8 within statistical uncertainties.

4.3   Correlation function parametrization

In the previous analyses performed by the ALICE Collaboration in pp collisions, the Gaussian distribution of a particle source in the pair reference frame (PRF) was assumed for pions [30] and kaons [33]. In those cases, the fit was performed using the Bowler–Sinyukov formula [60, 61]

$$C(q_{\mathrm{inv}}) = N \left(1 - \lambda + \lambda K(r, q_{\mathrm{inv}}) \left(1 + \exp\left(-R_{\mathrm{inv}}^2 q_{\mathrm{inv}}^2 \right) \right) \right), \tag{5}$$

where N is a normalization coefficient and $K(r, q_{\mathrm{inv}})$ is the Coulomb function with a radius r defined as

$$K(r, q_{\mathrm{inv}}) = \frac{C(\mathrm{QS} + \mathrm{Coulomb})}{C(\mathrm{QS})}. \tag{6}$$
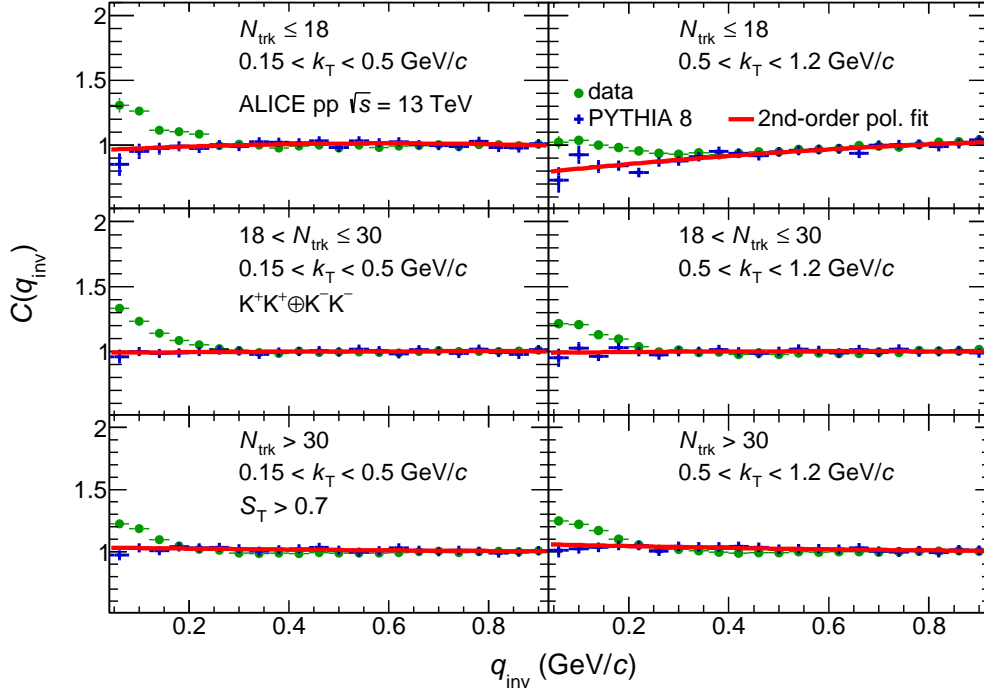
10

Figure 5: The $K^{\pm}K^{\pm}$ experimental correlation functions (green solid circles) as function of the invariant pair relative momentum q_{inv} in pp collisions at $\sqrt{s} = 13$ TeV for the raw multiplicity N_{trk} intervals of (1–18), (19–30), and (> 30) in the (0.15–0.5) GeV/c and (0.5–1.2) GeV/c k_T intervals. A sphericity selection of $S_T > 0.7$ is applied. The data are compared with PYTHIA 8 calculations shown by blue crosses. The PYTHIA 8 calculations are approximated with a second-order polynomial (red curves). The error bars represent the statistical uncertainties, while the systematic uncertainties are negligible.

The parameters R_{inv} and λ describe the size of the source and the correlation strength, respectively (see Eq. (5)). The term $C(\text{QS})$ in Eq. (6) is a theoretical CF calculated with pure QS weights (wave function squared) and $C(\text{QS}+\text{Coulomb})$ corresponds to QS+Coulomb weights. However, since the pion CFs are strongly non-Gaussian due to the large resonance contribution, an exponential Bowler–Sinyukov function was used to fit the pion CF like in Ref. [43]:

$$C(q_{inv}) = N(1 - \lambda + \lambda K(r, q_{inv})(1 + \exp(-R_{inv}q_{inv})))D(q_{inv}), \qquad (7)$$

where $D(q_{inv}) = bq_{inv} + 1$ accounts for the slope of the baseline which remains after the division by PYTHIA 8.

The measured pion CFs shown in Figs. 3–4 were divided by the PYTHIA 8 baseline and fit with the exponential Bowler–Sinyukov formula of Eq. (7). Figure 7 presents some examples of the pion CF fit with the Gaussian function of Eq. (5) (dotted line) and the exponential of Eq. (7) (solid line) Bowler–Sinyukov formulae. The exponential fit function describes the pion CF well both for spherical and jet-like events, although the description is not ideal for $q_{inv} < 0.05$ GeV/c.

The kaon CFs for spherical and jet-like events were corrected using a second-order polynomial to describe the non-femtoscopic background as explained above and fitted with the Gaussian Bowler–Sinyukov formula (Eq. (5)). An example of such a fit is shown in Fig. 8 both for spherical and jet-like events. For the largest multiplicity bin for $S_T < 0.3$ selection, kaon CFs do not exhibit any femtoscopic peak after the correction for the baseline and, therefore, the fit was not performed.
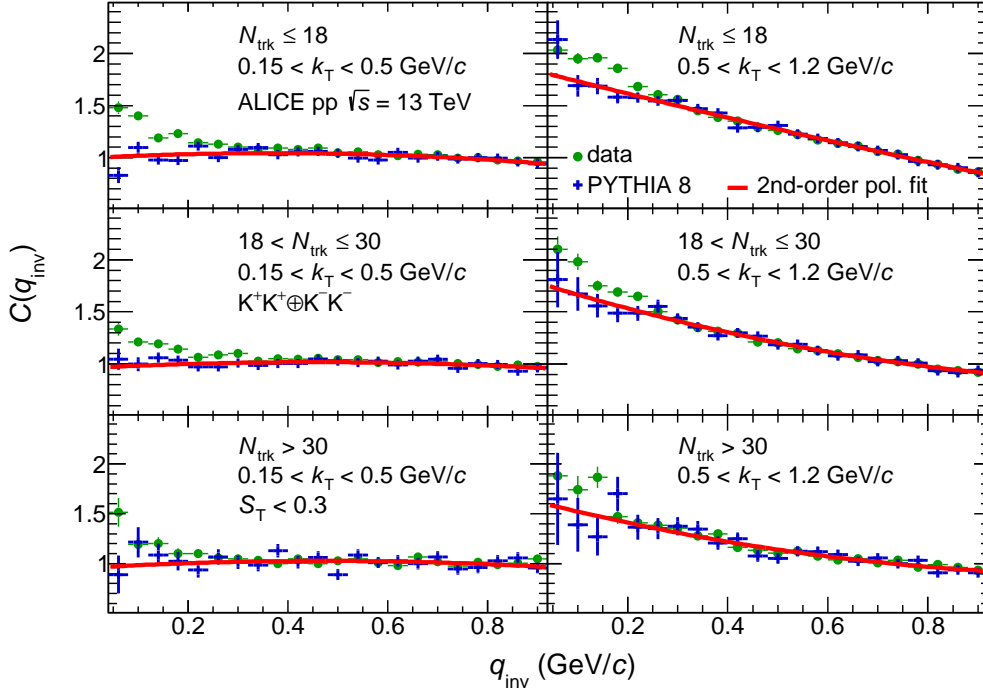
11

Figure 6: The $K^{\pm}K^{\pm}$ experimental correlation functions (green solid circles) as function of the invariant pair relative momentum q_{inv} in pp collisions at $\sqrt{s} = 13$ TeV for the raw multiplicity N_{trk} intervals of (1–18), (19–30), and (> 30) in the (0.15–0.5) GeV/c and (0.5–1.2) GeV/c k_T intervals. A sphericity selection of $S_T < 0.3$ is applied. The data are compared with PYTHIA 8 calculations, shown by blue crosses and approximated with a second-order polynomial (red curves). The error bars represent the statistical uncertainties, while the systematic uncertainties are negligible.

4.4   Systematic uncertainties

In this section, the systematic uncertainties estimated for the extracted source parameters R_{inv} and λ for $\pi^{\pm}\pi^{\pm}$ and $K^{\pm}K^{\pm}$ correlations at different sphericities are discussed.

The systematic uncertainty contributions related to particle selection and fit criteria $\Delta_{sys} = |y_0 - y_{var}|$ were considered, taking into account their statistical significance level determined by the Barlow factor [62]

$$B = \frac{|y_0 - y_{var}|}{\sqrt{\sigma_0^2 + \sigma_{var}^2 - 2\rho\,\sigma_0\sigma_{var}}}, \tag{8}$$

where y_0 is the default value, y_{var} is a value obtained with some variation of either the selection criteria or fit conditions, σ_0 is the statistical uncertainty of the default value, σ_{var} is the statistical uncertainty of the femtoscopic parameters obtained using varied analysis criteria, ρ characterizes the correlation between y_0 and y_{var}.

The systematic uncertainty contribution is taken into account if $B > 1$, i.e. only systematic uncertainties whose statistical significance level exceeds 68% are included in the total systematic uncertainty value. The systematic uncertainties Δ_{sys}^i corresponding to each ith variation of the particle selection and fit criteria and having $B > 1$ were added in quadrature to give the total systematic uncertainty Δ value

$$\Delta_{sys} = \sqrt{\sum_i \left(\Delta_{sys}^i\right)^2}. \tag{9}$$
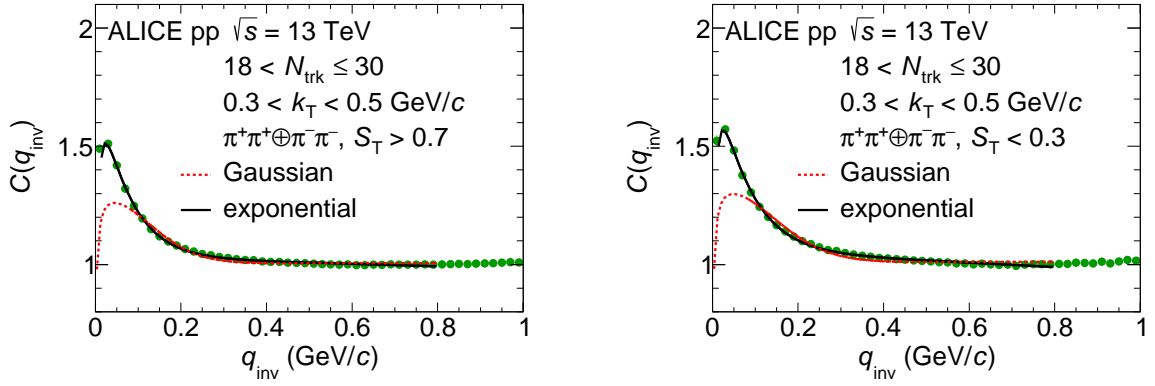
12

Figure 7: Examples of the pion CFs fitted with the Gaussian Eq. (5) (dotted line) and the exponential (solid line) Bowler–Sinyukov Eq. (7) formulae for spherical (left panel) and jet-like (right panel) events. Only statistical uncertainties are shown. Systematic uncertainties are negligible.
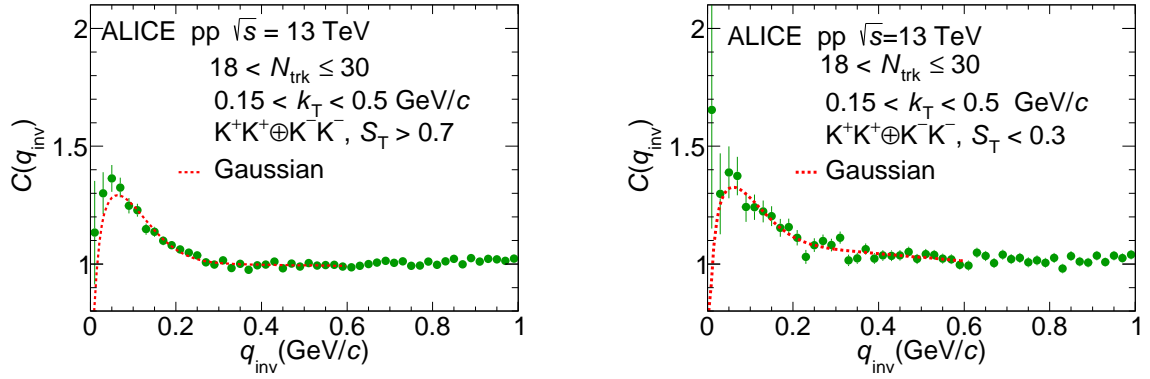

Figure 8: Examples of the kaon CFs fitted with the Gaussian Eq. (5) (dotted line) Bowler–Sinyukov formula for spherical (left panel) and jet-like (right panel) events. Only statistical uncertainties are shown. Systematic uncertainties are negligible.

As event selection criterion variation, the sphericity intervals were varied by ± 0.05 [43], resulting in a systematic uncertainty of up to 10% for the radii and λ parameters for pions and kaons.

The systematic uncertainties related to the track selection (p_T and η intervals, $\mathrm{DCA_{transverse}}$, $\mathrm{DCA_{longitudinal}}$, the values of the number of track points in TPC) were estimated by varying each selection criterion (see Tables 1 and 2) with variation limits up to $\pm 20\%$. Another source of systematic uncertainty is the misidentification of particles and the associated purity correction. The same $\pm 20\%$ variation of the parameters $n_{\sigma_{TPC}}$ and $n_{\sigma_{TOF}}$ used for the purity correction estimation was performed. The purity correction influences only the λ parameter. For pions, single particle purity is $\sim 99\%$ at $p < 1.5$ GeV/c, so the correction for purity is negligible. For kaons, it is $< 1\%$. The estimated systematic uncertainty for pions for spherical events is 2–5% for R_{inv} and λ, while for jet-like events it is 1–15% for R_{inv} and 1–20% for λ. For kaons, it is $< 5\%$ for spherical events, and 10–20% for jet-like events for both R_{inv} and λ.

To minimize the influence of two-track effects, the tracks in this analysis were required to have the average TPC separation of at least 3 cm. The systematic uncertainty related to these effects was estimated from comparing the resulting femtoscopic parameters with those obtained with the average TPC separation up to 10 cm. This comparison showed that the influence of the two-track effects on the extracted parameters was negligible.

It is known that usually the extracted femtoscopic parameters noticeably depend on the fit range if the baseline is not flat, which is the case for CF in pp collisions. To estimate the related systematic

13

uncertainty, three different fit ranges are considered: the standard $0 < q_{inv} < 0.8$ GeV/c, the shorter $0 < q_{inv} < 0.7$ GeV/c, and the longer $0 < q_{inv} < 0.9$ GeV/c ones. The systematic uncertainty for pion and kaon due to the variation in fit range is 1–12% for R_{inv} and 5–20% for λ.

The Coulomb interaction, described by the factor K in Eq. (6), is included in the default fitting procedure (Eqs. (5)–(7)). The influence of strong interactions on the extracted femtoscopic observables is estimated using the factor $K(q_{inv}) = C(\text{QS} + \text{Coulomb} + \text{strong})/C(\text{QS})$ and is taken as a systematic uncertainty. The strong interaction for both pions and kaons was calculated using the fully dynamical lattice QCD result [63]. The resulting systematic uncertainty for pions is 3–7% for R_{inv} and λ for both spherical and jet-like events. The systematic uncertainty related to the strong interactions for kaons is 7–15% for radii and correlation strengths for both spherical and jet-like events.

The systematic uncertainty introduced by the fit range variation was the only one observed to be fully correlated. For this uncertainty $\rho = 1$ in Eq. (8), while for all other uncertainties $\rho = 0$ was used.

5   Results and discussion

One of the goals of this work is to compare the kaon and pion radii for spherical and jet-like events in order to understand if the extracted radii follow the same m_T scaling behavior as observed in heavy-ion collisions.

To compare the strongly non-Gaussian pion source with the Gaussian kaon one, the exponential pion radii have to be converted to a Gaussian form. The Gaussian parametrization assumes a radial Gaussian distribution with the first moment of the distribution $1/R\sqrt{\pi}$, while the exponential parametrization assumes a Lorentzian one with the first moment of distribution $1/R$. Therefore, in order to compare the radii, the exponential radii should be divided by $\sqrt{\pi}$.
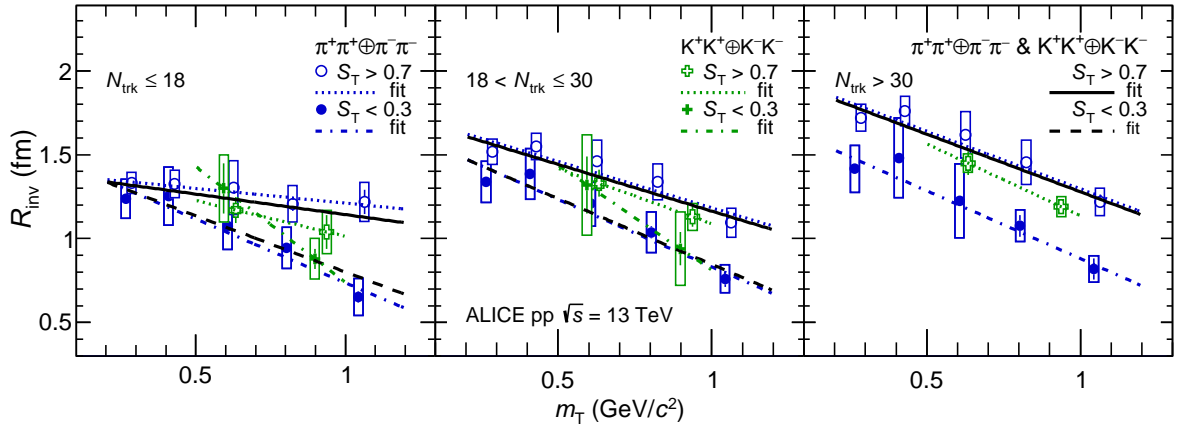

Figure 9: The Gaussian pion (blue circles) and kaon (green crosses) radii for spherical ($S_T > 0.7$) and jet-like ($S_T < 0.3$) events as function of the average pair transverse mass m_T for different multiplicity intervals. The lines approximating the pion and kaon radii by the linear function of Eq. (10) are shown for spherical events by dotted blue and green lines, respectively, and for jet-like events by dotted-dashed lines. The lines for combined fit for pion and kaon points are shown by black solid and dashed lines for spherical and jet-like events, respectively. Statistical (bars) and systematic (boxes) uncertainties are shown.

Figure 9 presents the m_T dependence of Gaussian radii for spherical and jet-like events for pions and kaons in different raw multiplicity intervals. As discussed in Section 4.2.1, the pion radii for $S_T > 0.7$, $N_{trk} < 18$ and $k_T > 0.50$ GeV/c ($m_T > 0.52$ GeV/c^2) have to be interpreted with caution because the baseline used to describe the non-femtoscopic effects was distorted at low q_{inv} (see Fig. 3) by the
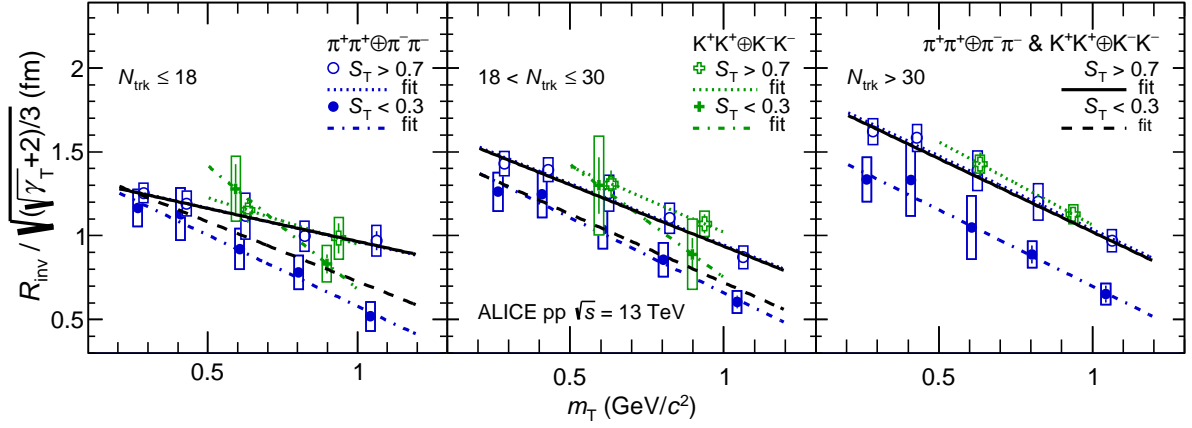
Figure 10: The Gaussian pion (blue circles) and kaon (green crosses) radii for spherical ($S_T > 0.7$) and jet-like ($S_T < 0.3$) events corrected for the Lorenz boost with factor in Eq. (11) as function of the average pair transverse mass m_T for different multiplicity intervals. The lines approximating the pion and kaon radii by the linear function of Eq. (10) are shown for spherical events by dotted blue and green lines, respectively, and for jet-like events by dotted-dashed lines. The lines for combined fit for pion and kaon points are shown by black solid and dashed lines for spherical and jet-like events, respectively. Statistical (bars) and systematic (boxes) uncertainties are shown.

$p_T > 0.5$ GeV/c three-track requirement requested for the calculation of the transverse sphericity.

The pion and kaon radii for spherical and jet-like events (Figures 9 and 10) were fitted in each multiplicity interval with a linear function

$$f(m_T) = a + bm_T, \qquad (10)$$

where a and b are free parameters. The results of this fitting are presented in Tables 4 and 5. The individual fits for pions and kaons are compared with the combined fit of pion and kaon radii. It should be noted that for kaons the line is not exactly a fit since there are only two points available but it illustrates the slope of the radii with m_T. It allows quantifying how much the kaon radius data points deviate from this fit and, thus, how well the approximate m_T scaling manifests itself. Both the spherical ($S_T > 0.7$) and the jet-like ($S_T < 0.3$) radii for pions and kaons decrease with increasing m_T. The statistical uncertainties are large, especially for kaons, but there is an indication that the spherical radii demonstrate a flatter dependence compared to the jet-like ones for $N_{trk} < 30$, while a more pronounced slope appears for $N_{trk} > 30$ (see Table 4). The spherical kaon radii are smaller than the corresponding spherical pion radii, and the difference increases with increasing multiplicity. The jet-like pion radii are smaller than spherical ones, and the difference increases with increasing multiplicity.

The m_T scaling for pions and kaons was predicted in a case of negligible transverse flow and common freeze-out for 3D radii in the Longitudinally Co-Moving System (LCMS) [26]), where the pair relative momentum is decomposed over (q_{out}, q_{side}, q_{long}). Here, the "long" component goes along the beam direction, "out" – along the pair transverse momentum, and "side" – perpendicular to the latter in the transverse plane, while the longitudinal total pair momentum vanishes. Theoretical calculations within the 3+1D hydrodynamic model coupled with the statistical hadronization code THERMINATOR-2 taking into account the resonance contribution showed an effective power-law scaling of 3D LCMS radii over the pair transverse mass for pions, kaons and protons [25]. The same scaling was also observed in Ref. [25] for the one-dimensional radii in the RPF. However, it is often challenging to do measurements in the LCMS due to limited number of events and, therefore, the measurements are performed in the PRF and then transformed from the PRF to the LCMS by applying a Lorentz boost in the direction of the pair transverse momentum with velocity $\beta_T = p_T/m_T$ as $\gamma_T R_{out}$ (where $\gamma_T = \sqrt{1 - \beta_T^2}$). Therefore,

15

Table 4: The parameters of the approximation by the linear function of Eq. 10 of the femtoscopic radii in PRF calculated for pions and kaons for spherical and jet-like events, as a function of pair transverse mass for the different multiplicity intervals from Figure 9.

type of fit	N_{trk}	b	a	χ^2/NDF
	3(1)–18	-0.18 ± 0.16	1.39 ± 0.09	0.18/3
pions, spherical events	19–30	-0.55 ± 0.14	1.74 ± 0.09	1.95/3
	> 30	-0.69 ± 0.14	1.98 ± 0.10	1.77/3
	3(1)–18	-0.76 ± 0.20	1.50 ± 0.14	0.90/3
pions, jet-like events	19–30	-0.80 ± 0.14	1.64 ± 0.14	1.2/3
	> 30	-0.81 ± 0.21	1.69 ± 0.17	0.63/3
	3(1)–18	-0.43 ± 0.60	1.44 ± 0.42	-
kaons, spherical events	19–30	-0.66 ± 0.43	1.75 ± 0.34	-
	> 30	-0.85 ± 0.38	1.99 ± 0.31	-
	3(1)–18	-1.38 ± 0.93	2.12 ± 0.78	-
kaons, jet-like events	19–30	-1.25 ± 1.38	2.06 ± 1.12	-
	> 30	-	-	-
	3(1)–18	-0.24 ± 0.15	1.39 ± 0.09	2.10/5
pions and kaons, spherical events	19–30	-0.56 ± 0.14	1.72 ± 0.09	2.25/5
	> 30	-0.69 ± 0.14	1.97 ± 0.09	2.00/5
	3(1)–18	-0.67 ± 0.16	1.47 ± 0.14	1.60/5
pions and kaons, jet-like events	19–30	-0.78 ± 0.17	1.63 ± 0.14	1.30/5
	> 30	-	-	-

the transverse (out) component of the 3D radius changes differently for pions and for kaons due to the different Lorentz boosts. In Ref. [25], it was shown that the scaling could be restored if the radii were divided by the following scaling factor

$$ f = \sqrt{(\sqrt{\gamma}_{\mathrm{T}} + 2)/3}. \tag{11} $$

After applying these kinematic corrections (Eq. (11)), the authors of Ref. [25] observed that the one-dimensional R_{inv} correlation radii for pions, kaons, and protons, as measured by ALICE in Pb–Pb collisions at $\sqrt{s_{\mathrm{NN}}}$ = 2.76 TeV [35], lied on a common curve (with the accuracy of 10%).

By applying this correction to the radii measured in this work (Fig. 10), the extracted pion and kaon radii for spherical events become closer to each other than in the case without such correction (Figure 9) considered above. The large uncertainties for kaon radii do not allow making any conclusion about the m_{T} scaling in jet-like events. The understanding of the m_{T} trend of the jet-like pion and kaon radii requires further study. The radii shown in Figure 10 were also fitted with the linear function of Eq. 10 (see Table 5). The χ^2/NDF for the fit of the uncorrected radii (Table 4) are larger than for the corrected ones (Table 5) for spherical events in all multiplicity intervals. This suggests an approximate m_{T} scaling for the radii for spherical events if the differences in Lorentz boosts for pions and kaons are taken into account.

It is also instructive to consider the difference between the radii with and without sphericity selection, as shown in Figure 11 for the pion radii for $S_{\mathrm{T}} > 0.7$, $S_{\mathrm{T}} < 0.3$, and without a selection on sphericity. It can be seen that for large multiplicities ($N_{\mathrm{trk}} > 18$) the radii extracted from the data without sphericity selections are close to those obtained in spherical events. This can be naturally explained by the experimental sphericity distributions presented in Fig. 1. The figure shows that all events tend to have large value of S_{T} and that the high-multiplicity intervals consist mainly of events with $S_{\mathrm{T}} > 0.7$. Therefore, the corresponding radii are close to each other within uncertainties. For $N_{\mathrm{trk}} < 18$ interval, the fraction

Table 5: The parameters of the approximation by the linear function of Eq. 10 of the femtoscopic radii in the PRF calculated for pions and kaons for spherical and jet-like events, as function of pair transverse mass for the different multiplicity intervals from Figure 10.

type of fit	N_{trk}	b	a	χ^2/NDF
	3(1)–18	-0.40 ± 0.13	1.36 ± 0.08	0.24/3
pions, spherical events	19–30	-0.73 ± 0.12	1.68 ± 0.08	0.81/3
	> 30	-0.87 ± 0.12	1.91 ± 0.09	0.69/3
	3(1)–18	-0.85 ± 0.17	1.43 ± 0.13	0.39/3
pions, jet-like events	19–30	-0.90 ± 0.16	1.55 ± 0.12	0.51/3
	> 30	-0.91 ± 0.19	1.61 ± 0.15	0.27/3
	3(1)–18	-0.55 ± 0.56	1.50 ± 0.40	-
kaons, spherical events	19–30	-0.79 ± 0.42	1.81 ± 0.33	-
	> 30	-0.99 ± 0.37	2.05 ± 0.31	-
	3(1)–18	-1.47 ± 0.9	2.15 ± 0.76	-
kaons, jet-like events	19–30	-1.35 ± 1.35	2.10 ± 0.10	-
	> 30	-	-	-
	3(1)–18	-0.39 ± 0.13	1.36 ± 0.08	0.45/5
pions and kaons, spherical events	19–30	-0.70 ± 0.12	1.67 ± 0.08	1.25/5
	> 30	-0.87 ± 0.12	1.90 ± 0.09	0.75/5
	3(1)–18	-0.71 ± 0.14	1.44 ± 0.12	10.1/5
pions and kaons, jet-like events	19–30	-0.82 ± 0.15	1.54 ± 0.12	3.10/5
	> 30	-	-	-

of particles with $S_{\text{T}} < 0.3$ becomes large, and the radii calculated without sphericity selection for this multiplicity interval are in between the $S_{\text{T}} > 0.7$ and $S_{\text{T}} < 0.3$ sphericity selected results, reflecting some interplay between all sphericity selected contributions.

Figure 12 demonstrates the m_{T} dependence of the correlation strength parameters λ for pions and kaons both for spherical (left panel) and jet-like (right panel) events. The λ parameters for pions were converted to a Gaussian form by dividing them by $\sqrt{\pi}$ in the same way as was done for the radii (see the discussion in the beginning of this section). The obtained pion λ weakly decreases with increasing m_{T}, and this behavior is similar for both sphericity selections. The kaon λ parameters are close to the pion ones, and all of them are in the range of ∼0.4–0.5. The main factors that could decrease the λ parameters compared to the ideal case of unity are the non-Gaussian shape of CFs due to contribution of particles from short-lived (strongly decaying) and medium-lived (ω for pions, K_{S}^0 for kaons) resonances and the R_{inv} distortion in the PRF due to the Lorenz boost in the out direction resulting in values for R_{side} and R_{long} to be smaller than R_{out}. For pions, the λ values are also reduced due to long-lived resonances such as η and $\eta^{'}$.

The decrease of the pion and kaon sphericity integrated radii with increasing pair transverse mass in pp collisions was observed at LHC energies before as an indication of collective behaviour, originating from either initial- or final-state correlations. However, there was not even an approximate m_{T} scaling shown. The intriguing analogy with heavy-ion collisions was interpreted as a possibility of the collective behavior due to quark–gluon plasma formation [30, 33, 40, 41].

The study presented here demonstrates a similar decrease of radii for both spherical and jet-like events. There is an indication of an approximate m_{T} scaling of the radii for pions and kaons in spherical events if the kinematic correction for these particle species is taken into account. However, the fact that the decreasing m_{T} dependence and even the approximate m_{T} scaling are observed in all multiplicity intervals including the lowest ones suggests that this effect does not support the hypothesis of collective expansion
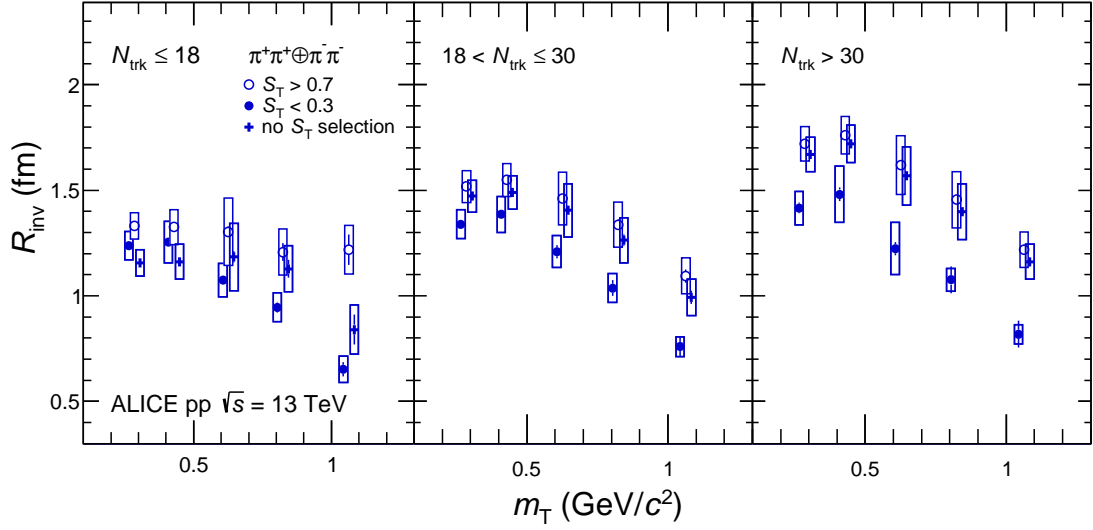
Figure 11: The Gaussian pion radii with $S_T > 0.7$ (open circles), $S_T < 0.3$ (solid circles) and without sphericity selection (solid crosses). Statistical (bars) and systematic (boxes) uncertainties are shown.

of hot and dense matter like in heavy-ion collisions. More realistic looks the hypothesis of common emission conditions for pions and kaons in pp collisions for the multiplicity intervals studied in this work, similar to the simplified scenario described in Ref. [25].

6 Summary

Correlations of two charged identical pions $\pi^{\pm}\pi^{\pm}$ and kaons $K^{\pm}K^{\pm}$ were measured in pp collisions at $\sqrt{s} = 13$ TeV at the LHC. One-dimensional pion and kaon correlations were classified using the global event-shape variable, transverse sphericity. For spherical events, the correlation functions show a strong suppression of mini-jet contributions. On the contrary, the correlation functions for jet-like events manifest large effects related to non-femtoscopic correlations at small relative momentum.

The Monte Carlo PYTHIA 8 (Monash) model describes both spherical and jet-like pion and kaon correlation functions outside the femtoscopic region effect. Therefore, it was used to subtract non-femtoscopic correlations from the femtoscopic signal region. The pion correlation functions corrected for mini-jet contributions as modeled by PYTHIA 8 are described by the exponential Bowler–Sinyukov function. The Bowler–Sinyukov function using a single Gaussian was used to describe the kaon correlations. The pion femtoscopic radii extracted for spherical events are larger than those for jet-like events. Both pion and kaon radii demonstrate a decreasing trend with increasing pair transverse mass m_T.

The Lorentz-boost corrected pion and kaon radii both for spherical and jet-like events show an approximate scaling behavior with m_T in all multiplicity intervals. The observation of such behavior for small multiplicity intervals, where the formation of QGP plasma seems to be impossible, can be interpreted as an indication of the emission occurring simultaneously for π and K in pp collisions for all considered multiplicities.

Acknowledgements
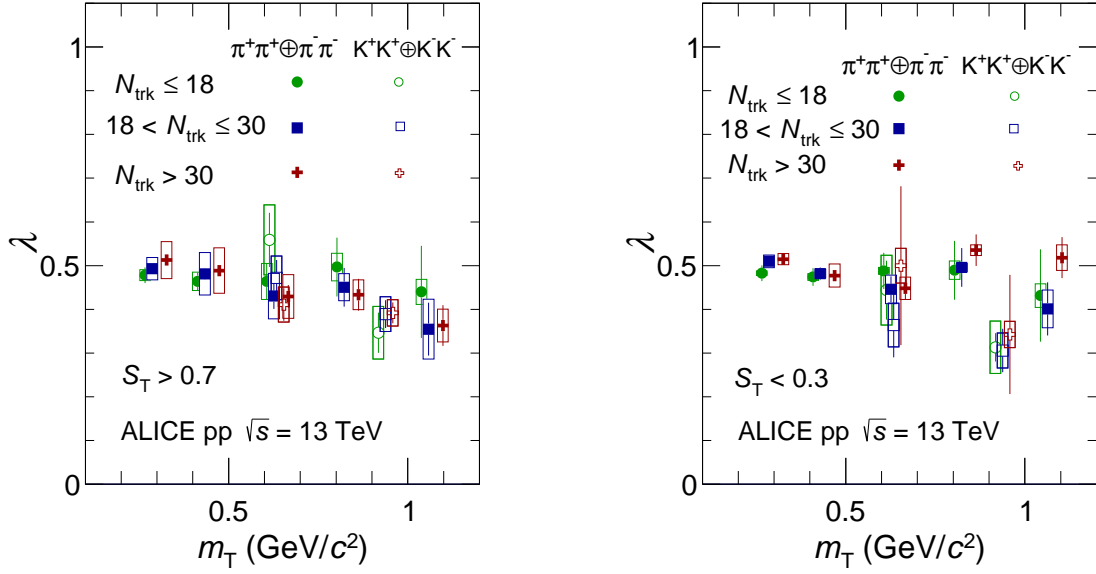
Figure 12: The Gaussian pion and kaon λ parameters for spherical (left panel) and jet-like (right panel) events as function of the average pair transverse mass m_T for different multiplicity intervals. The λ parameters are corrected for purity. Statistical (bars) and systematic (boxes) uncertainties are shown.

19

References

[1] J. L. Nagle and W. A. Zajc, "Small System Collectivity in Relativistic Hadronic and Nuclear Collisions", *Ann. Rev. Nucl. Part. Sci.* **68** (2018) 211–235, arXiv:1801.03477 [nucl-ex].

[2] J. Adolfsson *et al.*, "QCD challenges from pp to A–A collisions", *Eur. Phys. J. A* **56** (2020) 288, arXiv:2003.10997 [hep-ph].

[3] **ALICE** Collaboration, "The ALICE experiment - A journey through QCD", arXiv:2211.04384 [nucl-ex].

[4] **CMS** Collaboration, V. Khachatryan *et al.*, "Observation of Long-Range Near-Side Angular Correlations in Proton-Proton Collisions at the LHC", *JHEP* **09** (2010) 091, arXiv:1009.4122 [hep-ex].

[5] **ALICE** Collaboration, B. Abelev *et al.*, "Long-range angular correlations on the near and away side in p-Pb collisions at $\sqrt{s_{NN}} = 5.02$ TeV", *Phys. Lett. B* **719** (2013) 29–41, arXiv:1212.2001 [nucl-ex].

[6] **ATLAS** Collaboration, G. Aad *et al.*, "Observation of Long-Range Elliptic Azimuthal Anisotropies in $\sqrt{s} = 13$ and 2.76 TeV pp Collisions with the ATLAS Detector", *Phys. Rev. Lett.* **116** (2016) 172301, arXiv:1509.04776 [hep-ex].

[7] **ALICE** Collaboration, J. Adam *et al.*, "Enhanced production of multi-strange hadrons in high-multiplicity proton-proton collisions", *Nature Phys.* **13** (2017) 535–539, arXiv:1606.07424 [nucl-ex].

[8] T. Pierog, I. Karpenko, J. M. Katzy, E. Yatsenko, and K. Werner, "EPOS LHC: Test of collective hadronization with data measured at the CERN Large Hadron Collider", *Phys. Rev. C* **92** (2015) 034906, arXiv:1306.0121 [hep-ph].

[9] C. Bierlich, G. Gustafson, L. Lonnblad, and H. Shah, "The Angantyr model for Heavy-Ion Collisions in PYTHIA8", *JHEP* **10** (2018) 134, arXiv:1806.10820 [hep-ph].

[10] N. Fischer and T. Sjöstrand, "Thermodynamical String Fragmentation", *JHEP* **01** (2017) 140, arXiv:1610.09818 [hep-ph].

[11] W. Kittel, "Bose-Einstein correlations in Z fragmentation and other reactions", *Acta Phys.Polon.* **B32** (2001) 3927–3972, arXiv:hep-ph/0110088 [hep-ph].

[12] G. Alexander, "Bose-Einstein and Fermi-Dirac interferometry in particle physics", *Rept.Prog.Phys.* **66** (2003) 481–522, arXiv:hep-ph/0302130 [hep-ph].

[13] M. Podgoretsky, "Interference Correlations of Identical Pions: Theory", *Sov.J.Part.Nucl* **20** (1989) 266.

[14] R. Lednicky, "Correlation femtoscopy", *Nucl. Phys. A* **774** (2006) 189–198, arXiv:nucl-th/0510020.

[15] **STAR** Collaboration, B. I. Abelev *et al.*, "Pion Interferometry in Au+Au and Cu+Cu Collisions at RHIC", *Phys. Rev. C* **80** (2009) 024905, arXiv:0903.1296 [nucl-ex].

[16] **STAR** Collaboration, J. Adams *et al.*, "Pion interferometry in Au+Au collisions at S(NN)**(1/2) = 200-GeV", *Phys. Rev. C* **71** (2005) 044906, arXiv:nucl-ex/0411036.

[17] **PHOBOS** Collaboration, B. B. Back *et al.*, "Transverse momentum and rapidity dependence of HBT correlations in Au + Au collisions at s(NN)**(1/2) = 62.4-GeV and 200-GeV", *Phys. Rev. C* **73** (2006) 031901, arXiv:nucl-ex/0409001.

[18] **ALICE** Collaboration, K. Aamodt *et al.*, "Two-pion Bose-Einstein correlations in central Pb-Pb collisions at $\sqrt{s_{NN}}$ = 2.76 TeV", *Phys. Lett. B* **696** (2011) 328–337, arXiv:1012.4035 [nucl-ex].

[19] **ALICE** Collaboration, J. Adam *et al.*, "Centrality dependence of pion freeze-out radii in Pb-Pb collisions at $\sqrt{s_{NN}}$ = 2.76 TeV", *Phys. Rev. C* **93** (2016) 024905, arXiv:1507.06842 [nucl-ex].

[20] S. V. Akkelin and Y. M. Sinyukov, "The HBT interferometry of expanding sources", *Phys. Lett. B* **356** (1995) 525–530.

[21] I. A. Karpenko and Y. M. Sinyukov, "Energy dependence of pion interferometry scales in ultra-relativistic heavy ion collisions", *Phys. Lett. B* **688** (2010) 50–54, arXiv:0912.3457 [nucl-th].

[22] V. M. Shapoval, M. D. Adzhymambetov, and Y. M. Sinyukov, "Femtoscopy scales and particle production in the relativistic heavy ion collisions from Au+Au at 200 AGeV to Xe+Xe at 5.44 ATeV within the integrated hydrokinetic model", *Eur. Phys. J. A* **56** (2020) 260, arXiv:2006.16697 [nucl-th].

[23] A. Kisiel, T. Taluc, W. Broniowski, and W. Florkowski, "THERMINATOR: THERMal heavy-IoN generATOR", *Comput. Phys. Commun.* **174** (2006) 669–687, arXiv:nucl-th/0504047.

[24] P. Bozek, M. Chojnacki, W. Florkowski, and B. Tomasik, "Hydrodynamic predictions for Pb+Pb collisions at $\sqrt{S_{NN}}$ = 2.76 TeV", *Phys. Lett. B* **694** (2011) 238–241, arXiv:1007.2294 [nucl-th].

[25] A. Kisiel, M. Gałażyn, and P. Bożek, "Pion, kaon, and proton femtoscopy in Pb–Pb collisions at $\sqrt{s_{NN}}$=2.76 TeV modeled in (3+1)D hydrodynamics", *Phys. Rev. C* **90** (2014) 064914, arXiv:1409.4571 [nucl-th].

[26] A. N. Makhlin and Y. M. Sinyukov, "Hydrodynamics of Hadron Matter Under Pion Interferometric Microscope", *Z. Phys. C* **39** (1988) 69.

[27] V. M. Shapoval, P. Braun-Munzinger, I. A. Karpenko, and Y. M. Sinyukov, "Femtoscopy correlations of kaons in Pb+Pb collisions at LHC within hydrokinetic model", *Nucl. Phys. A* **929** (2014) 1–8, arXiv:1404.4501 [hep-ph].

[28] Y. M. Sinyukov, V. M. Shapoval, and V. Y. Naboka, "On m_T dependence of femtoscopy scales for meson and baryon pairs", *Nucl. Phys. A* **946** (2016) 227–239, arXiv:1508.01812 [hep-ph].

[29] **ALICE** Collaboration, S. Acharya *et al.*, "Kaon femtoscopy in Pb-Pb collisions at $\sqrt{s_{NN}} = 2.76$ TeV", *Phys. Rev. C* **96** (2017) 064613, arXiv:1709.01731 [nucl-ex].

[30] **ALICE** Collaboration, K. Aamodt *et al.*, "Femtoscopy of *pp* collisions at $\sqrt{s} = 0.9$ and 7 TeV at the LHC with two-pion Bose-Einstein correlations", *Phys. Rev. D* **84** (2011) 112004, arXiv:1101.3665 [hep-ex].

[31] **ALICE** Collaboration, J. Adam *et al.*, "Two-pion femtoscopy in p-Pb collisions at $\sqrt{s_{NN}} = 5.02$ TeV", *Phys. Rev. C* **91** (2015) 034906, arXiv:1502.00559 [nucl-ex].

[32] **ALICE** Collaboration, B. Abelev *et al.*, "$K_s^0 - K_s^0$ correlations in *pp* collisions at $\sqrt{s} = 7$ TeV from the LHC ALICE experiment", *Phys. Lett. B* **717** (2012) 151–161, arXiv:1206.2056 [hep-ex].

[33] **ALICE** Collaboration, B. Abelev *et al.*, "Charged kaon femtoscopic correlations in *pp* collisions at $\sqrt{s} = 7$ TeV", *Phys. Rev.* **D87** (2013) 052016, arXiv:1212.5958 [hep-ex].

[34] **ALICE** Collaboration, S. Acharya *et al.*, "One-dimensional charged kaon femtoscopy in p-Pb collisions at $\sqrt{s_{NN}} = 5.02$ TeV", *Phys. Rev. C* **100** (2019) 024002, arXiv:1903.12310 [nucl-ex].

[35] **ALICE** Collaboration, J. Adam *et al.*, "One-dimensional pion, kaon, and proton femtoscopy in Pb-Pb collisions at $\sqrt{s_{NN}} = 2.76$ TeV", *Phys. Rev.* **C92** (2015) 054908, arXiv:1506.07884 [nucl-ex].

[36] K. Werner, I. Karpenko, T. Pierog, M. Bleicher, and K. Mikhailov, "Evidence for hydrodynamic evolution in proton-proton scattering at 900 GeV", *Phys. Rev. C* **83** (2011) 044915, arXiv:1010.0400 [nucl-th].

[37] C. Plumberg, "Hanbury-Brown–Twiss interferometry and collectivity in $p+p$, p+Pb, and Pb+Pb collisions", *Phys. Rev. C* **102** (2020) 054908, arXiv:2008.01709 [nucl-th].

[38] V. M. Shapoval, P. Braun-Munzinger, I. A. Karpenko, and Y. M. Sinyukov, "Femtoscopic scales in $p+p$ and p+Pb collisions in view of the uncertainty principle", *Phys. Lett. B* **725** (2013) 139–147, arXiv:1304.3815 [hep-ph].

[39] M. S. Nilsson, L. V. Bravina, E. E. Zabrodin, L. V. Malinina, and J. Bleibel, "Study of $\pi\pi$ correlations at LHC and RHIC energies in *pp* collisions within the quark-gluon string model", *Phys. Rev. D* **84** (2011) 054006, arXiv:1106.1786 [hep-ph].

[40] **CMS** Collaboration, A. M. Sirunyan *et al.*, "Bose-Einstein correlations of charged hadrons in proton-proton collisions at $\sqrt{s} = 13$ TeV", *JHEP* **03** (2020) 014, arXiv:1910.08815 [hep-ex].

[41] **ATLAS** Collaboration, M. Aaboud *et al.*, "Femtoscopy with identified charged pions in proton-lead collisions at $\sqrt{s_{NN}} = 5.02$ TeV with ATLAS", *Phys. Rev. C* **96** (2017) 064908, arXiv:1704.01621 [hep-ex].

[42] **ALICE** Collaboration, B. Abelev *et al.*, "Freeze-out radii extracted from three-pion cumulants in pp, p–Pb and Pb–Pb collisions at the LHC", *Phys. Lett.* **B739** (2014) 139–151, `arXiv:1404.1194 [nucl-ex]`.

[43] **ALICE** Collaboration, S. Acharya *et al.*, "Event-shape and multiplicity dependence of freeze-out radii in pp collisions at $\sqrt{s} = 7$ TeV", *JHEP* **09** (2019) 108, `arXiv:1901.05518 [nucl-ex]`.

[44] **ALICE** Collaboration, B. Abelev *et al.*, "Transverse sphericity of primary charged particles in minimum bias proton-proton collisions at $\sqrt{s} = 0.9$, 2.76 and 7 TeV", *Eur. Phys. J.* **C72** (2012) 2124, `arXiv:1205.3963 [hep-ex]`.

[45] A. Banfi, G. P. Salam, and G. Zanderighi, "Resummed event shapes at hadron - hadron colliders", *JHEP* **08** (2004) 062, `arXiv:hep-ph/0407287`.

[46] A. Ortiz, G. Paić, and E. Cuautle, "Mid-rapidity charged hadron transverse spherocity in pp collisions simulated with Pythia", *Nucl. Phys. A* **941** (2015) 78–86, `arXiv:1503.03129 [hep-ph]`.

[47] **ALICE** Collaboration, S. Acharya *et al.*, "Charged-particle production as a function of multiplicity and transverse spherocity in pp collisions at $\sqrt{s} = 5.02$ and 13 TeV", *Eur. Phys. J. C* **79** (2019) 857, `arXiv:1905.07208 [nucl-ex]`.

[48] **ALICE** Collaboration, K. Aamodt *et al.*, "The ALICE experiment at the CERN LHC", *JINST* **3** (2008) S08002.

[49] **ALICE** Collaboration, B. Abelev *et al.*, "Performance of the ALICE experiment at the CERN LHC", *Int. J. Mod. Phys.* **A29** (2014) 1430044, `arXiv:1402.4476 [nucl-ex]`.

[50] **ALICE** Collaboration, K. Aamodt *et al.*, "Alignment of the ALICE Inner Tracking System with cosmic-ray tracks", *JINST* **5** (2010) P03003, `arXiv:1001.0502 [physics.ins-det]`.

[51] J. Alme *et al.*, "The ALICE TPC, a large 3-dimensional tracking device with fast readout for ultra-high multiplicity events", *Nucl. Instrum. Meth.* **A622** (2010) 316–367, `arXiv:1001.1950 [physics.ins-det]`.

[52] A. Akindinov *et al.*, "Performance of the ALICE Time-Of-Flight detector at the LHC", *Eur. Phys. J. Plus* **128** (2013) 44.

[53] **ALICE** Collaboration, E. Abbas *et al.*, "Performance of the ALICE VZERO system", *JINST* **8** (2013) P10016, `arXiv:1306.3130 [nucl-ex]`.

[54] **ALICE** Collaboration, S. Acharya *et al.*, "The ALICE definition of primary particles", *ALICE-PUBLIC-2017-005* (2017) .

[55] T. Sjöstrand, S. Ask, J. R. Christiansen, R. Corke, N. Desai, P. Ilten, S. Mrenna, S. Prestel, C. O. Rasmussen, and P. Z. Skands, "An introduction to PYTHIA 8.2", *Comput. Phys. Commun.* **191** (2015) 159–177, `arXiv:1410.3012 [hep-ph]`.

[56] P. Skands, S. Carrazza, and J. Rojo, "Tuning PYTHIA 8.1: the Monash 2013 Tune", *Eur. Phys. J. C* **74** (2014) 3024, `arXiv:1404.5630 [hep-ph]`.

[57] R. Brun, F. Bruyant, F. Carminati, S. Giani, M. Maire, A. McPherson, G. Patrick, and L. Urban, "GEANT Detector Description and Simulation Tool", *CERN-W5013, CERN-W-5013, W5013, W-5013* (10, 1994) .
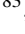
[58] **ALICE** Collaboration, B. Abelev *et al.*, "Transverse sphericity of primary charged particles in minimum bias proton-proton collisions at $\sqrt{s} = 0.9$, 2.76 and 7 TeV", *Eur. Phys. J. C* **72** (2012) 2124, `arXiv:1205.3963 [hep-ex]`.

[59] G. I. Kopylov, "Like particle correlations as a tool to study the multiple production mechanism", *Phys. Lett.* **B50** (1974) 472–474.

[60] Y. Sinyukov, R. Lednicky, S. Akkelin, J. Pluta, and B. Erazmus, "Coulomb corrections for interferometry analysis of expanding hadron systems", *Phys.Lett.* **B432** (1998) 248–257.

[61] M. Bowler, "Bose-Einstein Symmetrization: Coherence and Chaos: With Particular Application to $e^{+}e^{-}$ Annihilation", *Z.Phys.* **C29** (1985) 617.

[62] R. Barlow, "Systematic errors: Facts and fictions", in *Conference on Advanced Statistical Techniques in Particle Physics*, pp. 134–144. 7, 2002. `arXiv:hep-ex/0207026`.

[63] **NPLQCD** Collaboration, S. R. Beane, T. C. Luu, K. Orginos, A. Parreno, M. J. Savage, A. Torok, and A. Walker-Loud, "The $K^{+}K^{+}$ scattering length from lattice QCD", *Phys. Rev. D* **77** (2008) 094507, `arXiv:0709.1169 [hep-lat]`.

A   The ALICE Collaboration

S. Acharya [127], D. Adamová [86], G. Aglieri Rinella [33], M. Agnello [30], N. Agrawal [51], Z. Ahammed [135], S. Ahmad [16], S.U. Ahn [71], I. Ahuja [38], A. Akindinov [142], M. Al-Turany [97], D. Aleksandrov [142], B. Alessandro [56], H.M. Alfanda [6], R. Alfaro Molina [67], B. Ali [16], A. Alici [26], N. Alizadehvandchali [115], A. Alkin [33], J. Alme [21], G. Alocco [52], T. Alt [64], A.R. Altamura [50], I. Altsybeev [95], M.N. Anaam [6], C. Andrei [46], N. Andreou [114], A. Andronic [126], V. Anguelov [94], F. Antinori [54], P. Antonioli [51], N. Apadula [74], L. Aphecetche [103], H. Appelshäuser [64], C. Arata [73], S. Arcelli [26], M. Aresti [23], R. Arnaldi [56], J.G.M.C.A. Arneiro [110], I.C. Arsene [20], M. Arslandok [139], A. Augustinus [33], R. Averbeck [97], M.D. Azmi [16], H. Baba [123], A. Badalà [53], J. Bae [104], Y.W. Baek [41], X. Bai [119], R. Bailhache [64], Y. Bailung [48], A. Balbino [30], A. Baldisseri [130], B. Balis [2], D. Banerjee [4], Z. Banoo [91], R. Barbera [27], F. Barile [32], L. Barioglio [95], M. Barlou[78], B. Barman[42], G.G. Barnaföldi [138], L.S. Barnby [85], V. Barret [127], L. Barreto [110], C. Bartels [118], K. Barth [33], E. Bartsch [64], N. Bastid [127], S. Basu [75], G. Batigne [103], D. Battistini [95], B. Batyunya [143], D. Bauri[47], J.L. Bazo Alba [101], I.G. Bearden [83], C. Beattie [139], P. Becht [97], D. Behera [48], I. Belikov [129], A.D.C. Bell Hechavarria [126], F. Bellini [26], R. Bellwied [115], S. Belokurova [142], Y.A.V. Beltran [45], G. Bencedi [138], S. Beole [25], Y. Berdnikov [142], A. Berdnikova [94], L. Bergmann [94], M.G. Besoiu [63], L. Betev [33], P.P. Bhaduri [135], A. Bhasin [91], M.A. Bhat [4], B. Bhattacharjee [42], L. Bianchi [25], N. Bianchi [49], J. Bielčík [36], J. Bielčíková [86], J. Biernat [107], A.P. Bigot [129], A. Bilandzic [95], G. Biro [138], S. Biswas [4], N. Bize [103], J.T. Blair [108], D. Blau [142], M.B. Blidaru [97], N. Bluhme[39], C. Blume [64], G. Boca [22,55], F. Bock [87], T. Bodova [21], A. Bogdanov[142], S. Boi [23], J. Bok [58], L. Boldizsár [138], M. Bombara [38], P.M. Bond [33], G. Bonomi [134,55], H. Borel [130], A. Borissov [142], A.G. Borquez Carcamo [94], H. Bossi [139], E. Botta [25], Y.E.M. Bouziani [64], L. Bratrud [64], P. Braun-Munzinger [97], M. Bregant [110], M. Broz [36], G.E. Bruno [96,32], M.D. Buckland [24], D. Budnikov [142], H. Buesching [64], S. Bufalino [30], P. Buhler [102], N. Burmasov [142], Z. Buthelezi [68,122], A. Bylinkin [21], S.A. Bysiak[107], M. Cai [6], H. Caines [139], A. Caliva [29], E. Calvo Villar [101], J.M.M. Camacho [109], P. Camerini [24], F.D.M. Canedo [110], M. Carabas [125], A.A. Carballo [33], F. Carnesecchi [33], R. Caron [128], L.A.D. Carvalho [110], J. Castillo Castellanos [130], F. Catalano [33,25], C. Ceballos Sanchez [143], I. Chakaberia [74], P. Chakraborty [47], S. Chandra [135], S. Chapeland [33], M. Chartier [118], S. Chattopadhyay [135], S. Chattopadhyay [99], T.G. Chavez [45], T. Cheng [97,6], C. Cheshkov [128], B. Cheynis [128], V. Chibante Barroso [33], D.D. Chinellato [111], E.S. Chizzali [II,95], J. Cho [58], S. Cho [58], P. Chochula [33], D. Choudhury[42], P. Christakoglou [84], C.H. Christensen [83], P. Christiansen [75], T. Chujo [124], M. Ciacco [30], C. Cicalo [52], F. Cindolo [51], M.R. Ciupek[97], G. Clai[III,51], F. Colamaria [50], J.S. Colburn[100], D. Colella [96,32], M. Colocci [26], M. Concas [IV,33], G. Conesa Balbastre [73], Z. Conesa del Valle [131], G. Contin [24], J.G. Contreras [36], M.L. Coquet [130], P. Cortese [133,56], M.R. Cosentino [112], F. Costa [33], S. Costanza [22,55], C. Cot [131], J. Crkovská [94], P. Crochet [127], R. Cruz-Torres [74], P. Cui [6], A. Dainese [54], M.C. Danisch [94], A. Danu [63], P. Das [80], P. Das [4], S. Das [4], A.R. Dash [126], S. Dash [47], R.M.H. David[45], A. De Caro [29], G. de Cataldo [50], J. de Cuveland[39], A. De Falco [23], D. De Gruttola [29], N. De Marco [56], C. De Martin [24], S. De Pasquale [29], R. Deb [134], R. Del Grande [95], L. Dello Stritto [29], W. Deng [6], P. Dhankher [19], D. Di Bari [32], A. Di Mauro [33], B. Diab [130], R.A. Diaz [143,7], T. Dietel [113], Y. Ding [6], J. Ditzel [64], R. Divià [33], D.U. Dixit [19], Ø. Djuvsland[21], U. Dmitrieva [142], A. Dobrin [63], B. Dönigus [64], J.M. Dubinski [136], A. Dubla [97], S. Dudi [90], P. Dupieux [127], M. Durkac[106], N. Dzalaiova[13], T.M. Eder [126], R.J. Ehlers [74], F. Eisenhut [64], R. Ejima[92], D. Elia [50], B. Erazmus [103], F. Ercolessi [26], F. Erhardt [89], M.R. Ersdal[21], B. Espagnon [131], G. Eulisse [33], D. Evans [100], S. Evdokimov [142], L. Fabbietti [95], M. Faggin [28], J. Faivre [73], F. Fan [6], W. Fan [74], A. Fantoni [49], M. Fasel [87], A. Feliciello [56], G. Feofilov [142], A. Fernández Téllez [45], L. Ferrandi [110], M.B. Ferrer [33], A. Ferrero [130], C. Ferrero [56], A. Ferretti [25], V.J.G. Feuillard [94], V. Filova [36], D. Finogeev [142], F.M. Fionda [52], F. Flor [115], A.N. Flores [108], S. Foertsch [68], I. Fokin [94], S. Fokin [142], E. Fragiacomo [57], E. Frajna [138], U. Fuchs [33], N. Funicello [29], C. Furget [73], A. Furs [142], T. Fusayasu [98], J.J. Gaardhøje [83], M. Gagliardi [25], A.M. Gago [101], T. Gahlaut[47], C.D. Galvan [109], D.R. Gangadharan [115], P. Ganoti [78], C. Garabatos [97], A.T. Garcia [131], J.R.A. Garcia [45], E. Garcia-Solis [9], C. Gargiulo [33], P. Gasik [97], A. Gautam [117], M.B. Gay Ducati [66], M. Germain [103], A. Ghimouz[124], C. Ghosh[135], M. Giacalone [51], G. Gioachin [30], P. Giubellino [97,56], P. Giubilato [28], A.M.C. Glaenzer [130], P. Glässel [94], E. Glimos [121], D.J.Q. Goh[76], V. Gonzalez [137], M. Gorgon [2], K. Goswami [48], S. Gotovac[34], V. Grabski [67], L.K. Graczykowski [136], E. Grecka [86], A. Grelli [59], C. Grigoras [33], V. Grigoriev [142], S. Grigoryan [143,1], F. Grosa [33], J.F. Grosse-Oetringhaus [33], R. Grosso [97], D. Grund [36], N.A. Grunwald[94], G.G. Guardiano [111], R. Guernane [73], M. Guilbaud [103],

K. Gulbrandsen [83], T. Gündem [64], T. Gunji [123], W. Guo [6], A. Gupta [91], R. Gupta [91], R. Gupta [48], S.P. Guzman [45], K. Gwizdziel [136], L. Gyulai [138], C. Hadjidakis [131], F.U. Haider [91], S. Haidlova [36], H. Hamagaki [76], A. Hamdi [74], Y. Han [140], B.G. Hanley [137], R. Hannigan [108], J. Hansen [75], M.R. Haque [136], J.W. Harris [139], A. Harton [9], H. Hassan [116], D. Hatzifotiadou [51], P. Hauer [43], L.B. Havener [139], S.T. Heckel [95], E. Hellbär [97], H. Helstrup [35], M. Hemmer [64], T. Herman [36], G. Herrera Corral [8], F. Herrmann [126], S. Herrmann [128], K.F. Hetland [35], B. Heybeck [64], H. Hillemanns [33], B. Hippolyte [129], F.W. Hoffmann [70], B. Hofman [59], G.H. Hong [140], M. Horst [95], A. Horzyk [2], Y. Hou [6], P. Hristov [33], C. Hughes [121], P. Huhn [64], L.M. Huhta [116], T.J. Humanic [88], A. Hutson [115], D. Hutter [39], R. Ilkaev [142], H. Ilyas [14], M. Inaba [124], G.M. Innocenti [33], M. Ippolitov [142], A. Isakov [84,86], T. Isidori [117], M.S. Islam [99], M. Ivanov [13], M. Ivanov [97], V. Ivanov [142], K.E. Iversen [75], M. Jablonski [2], B. Jacak [74], N. Jacazio [26], P.M. Jacobs [74], S. Jadlovska [106], J. Jadlovsky [106], S. Jaelani [82], C. Jahnke [111], M.J. Jakubowska [136], M.A. Janik [136], T. Janson [70], S. Ji [17], S. Jia [10], A.A.P. Jimenez [65], F. Jonas [87], D.M. Jones [118], J.M. Jowett [33,97], J. Jung [64], M. Jung [64], A. Junique [33], A. Jusko [100], M.J. Kabus [33,136], J. Kaewjai [105], P. Kalinak [60], A.S. Kalteyer [97], A. Kalweit [33], V. Kaplin [142], A. Karasu Uysal [72], D. Karatovic [89], O. Karavichev [142], T. Karavicheva [142], P. Karczmarczyk [136], E. Karpechev [142], U. Kebschull [70], R. Keidel [141], D.L.D. Keijdener [59], M. Keil [33], B. Ketzer [43], S.S. Khade [48], A.M. Khan [119,6], S. Khan [16], A. Khanzadeev [142], Y. Kharlov [142], A. Khatun [117], A. Khuntia [36], B. Kileng [35], B. Kim [104], C. Kim [17], D.J. Kim [116], E.J. Kim [69], J. Kim [140], J.S. Kim [41], J. Kim [58], J. Kim [69], M. Kim [19], S. Kim [18], T. Kim [140], K. Kimura [92], S. Kirsch [64], I. Kisel [39], S. Kiselev [142], A. Kisiel [136], J.P. Kitowski [2], J.L. Klay [5], J. Klein [33], S. Klein [74], C. Klein-Bösing [126], M. Kleiner [64], T. Klemenz [95], A. Kluge [33], A.G. Knospe [115], C. Kobdaj [105], T. Kollegger [97], A. Kondratyev [143], N. Kondratyeva [142], E. Kondratyuk [142], J. Konig [64], S.A. Konigstorfer [95], P.J. Konopka [33], G. Kornakov [136], M. Korwieser [95], S.D. Koryciak [2], A. Kotliarov [86], V. Kovalenko [142], M. Kowalski [107], V. Kozhuharov [37], I. Králik [60], A. Kravčáková [38], L. Krcal [33,39], M. Krivda [100,60], F. Krizek [86], K. Krizkova Gajdosova [33], M. Kroesen [94], M. Krüger [64], D.M. Krupova [36], E. Kryshen [142], V. Kučera [58], C. Kuhn [129], P.G. Kuijer [84], T. Kumaoka [124], D. Kumar [135], L. Kumar [90], N. Kumar [90], S. Kumar [32], S. Kundu [33], P. Kurashvili [79], A. Kurepin [142], A.B. Kurepin [142], A. Kuryakin [142], S. Kushpil [86], M.J. Kweon [58], Y. Kwon [140], S.L. La Pointe [39], P. La Rocca [27], A. Lakrathok [105], M. Lamanna [33], A.R. Landou [73,114], R. Langoy [120], P. Larionov [33], E. Laudi [33], L. Lautner [33,95], R. Lavicka [102], R. Lea [134,55], H. Lee [104], I. Legrand [46], G. Legras [126], J. Lehrbach [39], T.M. Lelek [2], R.C. Lemmon [85], I. León Monzón [109], M.M. Lesch [95], E.D. Lesser [19], P. Lévai [138], X. Li [10], J. Lien [120], R. Lietava [100], I. Likmeta [115], B. Lim [25], S.H. Lim [17], V. Lindenstruth [39], A. Lindner [46], C. Lippmann [97], D.H. Liu [6], J. Liu [118], G.S.S. Liveraro [111], I.M. Lofnes [21], C. Loizides [87], S. Lokos [107], J. Lomker [59], P. Loncar [34], X. Lopez [127], E. López Torres [7], P. Lu [97,119], J.R. Luhder [126], M. Lunardon [28], G. Luparello [57], Y.G. Ma [40], M. Mager [33], A. Maire [129], M.V. Makariev [37], M. Malaev [142], G. Malfattore [26], N.M. Malik [91], Q.W. Malik [20], S.K. Malik [91], L. Malinina [I,VII,143], D. Mallick [131,80], N. Mallick [48], G. Mandaglio [31,53], S.K. Mandal [79], V. Manko [142], F. Manso [127], V. Manzari [50], Y. Mao [6], R.W. Marcjan [2], G.V. Margagliotti [24], A. Margotti [51], A. Marín [97], C. Markert [108], P. Martinengo [33], M.I. Martínez [45], G. Martínez García [103], M.P.P. Martins [110], S. Masciocchi [97], M. Masera [25], A. Masoni [52], L. Massacrier [131], O. Massen [59], A. Mastroserio [132,50], O. Matonoha [75], S. Mattiazzo [28], A. Matyja [107], C. Mayer [107], A.L. Mazuecos [33], F. Mazzaschi [25], M. Mazzilli [33], J.E. Mdhluli [122], Y. Melikyan [44], A. Menchaca-Rocha [67], E. Meninno [102,29], A.S. Menon [115], M. Meres [13], S. Mhlanga [113,68], Y. Miake [124], L. Micheletti [33], D.L. Mihaylov [95], K. Mikhaylov [143,142], A.N. Mishra [138], D. Miśkowiec [97], A. Modak [4], B. Mohanty [80], M. Mohisin Khan [V,16], M.A. Molander [44], S. Monira [136], C. Mordasini [116], D.A. Moreira De Godoy [126], I. Morozov [142], A. Morsch [33], T. Mrnjavac [33], V. Muccifora [49], S. Muhuri [135], J.D. Mulligan [74], A. Mulliri [23], M.G. Munhoz [110], R.H. Munzer [64], H. Murakami [123], S. Murray [113], L. Musa [33], J. Musinsky [60], J.W. Myrcha [136], B. Naik [122], A.I. Nambrath [19], B.K. Nandi [47], R. Nania [51], E. Nappi [50], A.F. Nassirpour [18], A. Nath [94], C. Nattrass [121], M.N. Naydenov [37], A. Neagu [20], A. Negru [125], L. Nellen [65], R. Nepeivoda [75], S. Nese [20], G. Neskovic [39], N. Nicassio [50], B.S. Nielsen [83], E.G. Nielsen [83], S. Nikolaev [142], S. Nikulin [142], V. Nikulin [142], F. Noferini [51], S. Noh [12], P. Nomokonov [143], J. Norman [118], N. Novitzky [124], P. Nowakowski [136], A. Nyanin [142], J. Nystrand [21], M. Ogino [76], S. Oh [18], A. Ohlson [75], V.A. Okorokov [142], J. Oleniacz [136], A.C. Oliveira Da Silva [121], A. Onnerstad [116], C. Oppedisano [56], A. Ortiz Velasquez [65], J. Otwinowski [107], M. Oya [92], K. Oyama [76], Y. Pachmayer [94], S. Padhan [47], D. Pagano [134,55], G. Paić [65], A. Palasciano [50], S. Panebianco [130], H. Park [124], H. Park [104], J. Park [58], J.E. Parkkila [33],

Y. Patley [47], R.N. Patra[91], B. Paul [23], H. Pei [6], T. Peitzmann [59], X. Peng [11], M. Pennisi [25],
S. Perciballi [25], D. Peresunko [142], G.M. Perez [7], Y. Pestov[142], V. Petrov [142], M. Petrovici [46],
R.P. Pezzi [103,66], S. Piano [57], M. Pikna [13], P. Pillot [103], O. Pinazza [51,33], L. Pinsky[115], C. Pinto [95],
S. Pisano [49], M. Płoskoń [74], M. Planinic[89], F. Pliquett[64], M.G. Poghosyan [87], B. Polichtchouk [142],
S. Politano [30], N. Poljak [89], A. Pop [46], S. Porteboeuf-Houssais [127], V. Pozdniakov [143], I.Y. Pozos [45],
K.K. Pradhan [48], S.K. Prasad [4], S. Prasad [48], R. Preghenella [51], F. Prino [56], C.A. Pruneau [137],
I. Pshenichnov [142], M. Puccio [33], S. Pucillo [25], Z. Pugelova[106], S. Qiu [84], L. Quaglia [25], S. Ragoni [15],
A. Rai [139], A. Rakotozafindrabe [130], L. Ramello [133,56], F. Rami [129], S.A.R. Ramirez [45], T.A. Rancien[73],
M. Rasa [27], S.S. Räsänen [44], R. Rath [51], M.P. Rauch [21], I. Ravasenga [84], K.F. Read [87,121],
C. Reckziegel [112], A.R. Redelbach [39], K. Redlich [VI,79], C.A. Reetz [97], A. Rehman[21], F. Reidt [33],
H.A. Reme-Ness [35], Z. Rescakova[38], K. Reygers [94], A. Riabov [142], V. Riabov [142], R. Ricci [29],
M. Richter [20], A.A. Riedel [95], W. Riegler [33], A.G. Riffero [25], C. Ristea [63], M.V. Rodriguez [33],
M. Rodríguez Cahuantzi [45], K. Røed [20], R. Rogalev [142], E. Rogochaya [143], T.S. Rogoschinski [64],
D. Rohr [33], D. Röhrich [21], P.F. Rojas[45], S. Rojas Torres [36], P.S. Rokita [136], G. Romanenko [26],
F. Ronchetti [49], A. Rosano [31,53], E.D. Rosas[65], K. Roslon [136], A. Rossi [54], A. Roy [48], S. Roy [47],
N. Rubini [26], D. Ruggiano [136], R. Rui [24], P.G. Russek [2], R. Russo [84], A. Rustamov [81],
E. Ryabinkin [142], Y. Ryabov [142], A. Rybicki [107], H. Rytkonen [116], J. Ryu [17], W. Rzesa [136],
O.A.M. Saarimaki [44], S. Sadhu [32], S. Sadovsky [142], J. Saetre [21], K. Šafařík [36], P. Saha[42], S.K. Saha [4],
S. Saha [80], B. Sahoo [47], B. Sahoo [48], R. Sahoo [48], S. Sahoo[61], D. Sahu [48], P.K. Sahu [61], J. Saini [135],
K. Sajdakova[38], S. Sakai [124], M.P. Salvan [97], S. Sambyal [91], D. Samitz [102], I. Sanna [33,95],
T.B. Saramela[110], P. Sarma [42], V. Sarritzu [23], V.M. Sarti [95], M.H.P. Sas [139], J. Schambach [87],
H.S. Scheid [64], C. Schiaua [46], R. Schicker [94], A. Schmah[97], C. Schmidt [97], H.R. Schmidt[93],
M.O. Schmidt [33], M. Schmidt[93], N.V. Schmidt [87], A.R. Schmier [121], R. Schotter [129], A. Schröter [39],
J. Schukraft [33], K. Schweda [97], G. Scioli [26], E. Scomparin [56], J.E. Seger [15], Y. Sekiguchi[123],
D. Sekihata [123], M. Selina [84], I. Selyuzhenkov [97], S. Senyukov [129], J.J. Seo [94,58], D. Serebryakov [142],
L. Šerkšnytė [95], A. Sevcenco [63], T.J. Shaba [68], A. Shabetai [103], R. Shahoyan[33], A. Shangaraev [142],
A. Sharma[90], B. Sharma [91], D. Sharma [47], H. Sharma [54,107], M. Sharma[91], S. Sharma [76], S. Sharma [91],
U. Sharma [91], A. Shatat [131], O. Sheibani[115], K. Shigaki [92], M. Shimomura[77], J. Shin[12], S. Shirinkin [142],
Q. Shou [40], Y. Sibiriak [142], S. Siddhanta [52], T. Siemiarczuk [79], T.F. Silva [110], D. Silvermyr [75],
T. Simantathammakul[105], R. Simeonov [37], B. Singh[91], B. Singh [95], K. Singh [48], R. Singh [80],
R. Singh [91], R. Singh [48], S. Singh [16], V.K. Singh [135], V. Singhal [135], T. Sinha [99], B. Sitar [13],
M. Sitta [133,56], T.B. Skaali[20], G. Skorodumovs [94], M. Slupecki [44], N. Smirnov [139], R.J.M. Snellings [59],
E.H. Solheim [20], J. Song [115], C. Sonnabend [33,97], F. Soramel [28], A.B. Soto-hernandez [88],
R. Spijkers [84], I. Sputowska [107], J. Staa [75], J. Stachel [94], I. Stan [63], P.J. Steffanic [121],
S.F. Stiefelmaier [94], D. Stocco [103], I. Storehaug [20], P. Stratmann [126], S. Strazzi [26], A. Sturniolo [31,53],
C.P. Stylianidis[84], A.A.P. Suaide [110], C. Suire [131], M. Sukhanov [142], M. Suljic [33], R. Sultanov [142],
V. Sumberia [91], S. Sumowidagdo [82], S. Swain[61], I. Szarka [13], M. Szymkowski [136], S.F. Taghavi [95],
G. Taillepied [97], J. Takahashi [111], G.J. Tambave [80], S. Tang [6], Z. Tang [119], J.D. Tapia Takaki [117],
N. Tapus[125], L.A. Tarasovicova [126], M.G. Tarzila [46], G.F. Tassielli [32], A. Tauro [33], G. Tejeda Muñoz [45],
A. Telesca [33], L. Terlizzi [25], C. Terrevoli [115], S. Thakur [4], D. Thomas [108], A. Tikhonov [142],
A.R. Timmins [115], M. Tkacik[106], T. Tkacik [106], A. Toia [64], R. Tokumoto[92], K. Tomohiro[92],
N. Topilskaya [142], M. Toppi [49], T. Tork [131], V.V. Torres [103], A.G. Torres Ramos [32], A. Trifiró [31,53],
A.S. Triolo [33,31,53], S. Tripathy [51], T. Tripathy [47], S. Trogolo [33], V. Trubnikov [3], W.H. Trzaska [116],
T.P. Trzcinski [136], A. Tumkin [142], R. Turrisi [54], T.S. Tveter [20], K. Ullaland [21], B. Ulukutlu [95],
A. Uras [128], G.L. Usai [23], M. Vala[38], N. Valle [22], L.V.R. van Doremalen[59], M. van Leeuwen [84], C.A. van
Veen [94], R.J.G. van Weelden [84], P. Vande Vyvre [33], D. Varga [138], Z. Varga [138], M. Vasileiou [78],
A. Vasiliev [142], O. Vázquez Doce [49], O. Vazquez Rueda [115], V. Vechernin [142], E. Vercellin [25], S. Vergara
Limón[45], R. Verma[47], L. Vermunt [97], R. Vértesi [138], M. Verweij [59], L. Vickovic[34], Z. Vilakazi[122],
O. Villalobos Baillie [100], A. Villani [24], A. Vinogradov [142], T. Virgili [29], M.M.O. Virta [116],
V. Vislavicius[75], A. Vodopyanov [143], B. Volkel [33], M.A. Völkl [94], K. Voloshin[142], S.A. Voloshin [137],
G. Volpe [32], B. von Haller [33], I. Vorobyev [95], N. Vozniuk [142], J. Vrláková [38], J. Wan[40], C. Wang [40],
D. Wang[40], Y. Wang [40], Y. Wang [6], A. Wegrzynek [33], F.T. Weiglhofer[39], S.C. Wenzel [33],
J.P. Wessels [126], S.L. Weyhmiller [139], J. Wiechula [64], J. Wikne [20], G. Wilk [79], J. Wilkinson [97],
G.A. Willems [126], B. Windelband [94], M. Winn [130], J.R. Wright [108], W. Wu[40], Y. Wu [119], R. Xu [6],
A. Yadav [43], A.K. Yadav [135], S. Yalcin [72], Y. Yamaguchi [92], S. Yang[21], S. Yano [92], Z. Yin [6],
I.-K. Yoo [17], J.H. Yoon [58], H. Yu[12], S. Yuan[21], A. Yuncu [94], V. Zaccolo [24], C. Zampolli [33],

27

F. Zanone [94], N. Zardoshti [33], A. Zarochentsev [142], P. Závada [62], N. Zaviyalov[142], M. Zhalov [142], B. Zhang [6], C. Zhang [130], L. Zhang [40], S. Zhang [40], X. Zhang [6], Y. Zhang[119], Z. Zhang [6], M. Zhao [10], V. Zherebchevskii [142], Y. Zhi[10], D. Zhou [6], Y. Zhou [83], J. Zhu [97,6], Y. Zhu[6], S.C. Zugravel [56], N. Zurlo [134,55]

Affiliation Notes

[I] Deceased
[II] Also at: Max-Planck-Institut für Physik, Munich, Germany
[III] Also at: Italian National Agency for New Technologies, Energy and Sustainable Economic Development (ENEA), Bologna, Italy
[IV] Also at: Dipartimento DET del Politecnico di Torino, Turin, Italy
[V] Also at: Department of Applied Physics, Aligarh Muslim University, Aligarh, India
[VI] Also at: Institute of Theoretical Physics, University of Wroclaw, Poland
[VII] Also at: An institution covered by a cooperation agreement with CERN

Collaboration Institutes

[1] A.I. Alikhanyan National Science Laboratory (Yerevan Physics Institute) Foundation, Yerevan, Armenia
[2] AGH University of Krakow, Cracow, Poland
[3] Bogolyubov Institute for Theoretical Physics, National Academy of Sciences of Ukraine, Kiev, Ukraine
[4] Bose Institute, Department of Physics and Centre for Astroparticle Physics and Space Science (CAPSS), Kolkata, India
[5] California Polytechnic State University, San Luis Obispo, California, United States
[6] Central China Normal University, Wuhan, China
[7] Centro de Aplicaciones Tecnológicas y Desarrollo Nuclear (CEADEN), Havana, Cuba
[8] Centro de Investigación y de Estudios Avanzados (CINVESTAV), Mexico City and Mérida, Mexico
[9] Chicago State University, Chicago, Illinois, United States
[10] China Institute of Atomic Energy, Beijing, China
[11] China University of Geosciences, Wuhan, China
[12] Chungbuk National University, Cheongju, Republic of Korea
[13] Comenius University Bratislava, Faculty of Mathematics, Physics and Informatics, Bratislava, Slovak Republic
[14] COMSATS University Islamabad, Islamabad, Pakistan
[15] Creighton University, Omaha, Nebraska, United States
[16] Department of Physics, Aligarh Muslim University, Aligarh, India
[17] Department of Physics, Pusan National University, Pusan, Republic of Korea
[18] Department of Physics, Sejong University, Seoul, Republic of Korea
[19] Department of Physics, University of California, Berkeley, California, United States
[20] Department of Physics, University of Oslo, Oslo, Norway
[21] Department of Physics and Technology, University of Bergen, Bergen, Norway
[22] Dipartimento di Fisica, Università di Pavia, Pavia, Italy
[23] Dipartimento di Fisica dell'Università and Sezione INFN, Cagliari, Italy
[24] Dipartimento di Fisica dell'Università and Sezione INFN, Trieste, Italy
[25] Dipartimento di Fisica dell'Università and Sezione INFN, Turin, Italy
[26] Dipartimento di Fisica e Astronomia dell'Università and Sezione INFN, Bologna, Italy
[27] Dipartimento di Fisica e Astronomia dell'Università and Sezione INFN, Catania, Italy
[28] Dipartimento di Fisica e Astronomia dell'Università and Sezione INFN, Padova, Italy
[29] Dipartimento di Fisica 'E.R. Caianiello' dell'Università and Gruppo Collegato INFN, Salerno, Italy
[30] Dipartimento DISAT del Politecnico and Sezione INFN, Turin, Italy
[31] Dipartimento di Scienze MIFT, Università di Messina, Messina, Italy
[32] Dipartimento Interateneo di Fisica 'M. Merlin' and Sezione INFN, Bari, Italy
[33] European Organization for Nuclear Research (CERN), Geneva, Switzerland
[34] Faculty of Electrical Engineering, Mechanical Engineering and Naval Architecture, University of Split, Split, Croatia
[35] Faculty of Engineering and Science, Western Norway University of Applied Sciences, Bergen, Norway

[36] Faculty of Nuclear Sciences and Physical Engineering, Czech Technical University in Prague, Prague, Czech Republic
[37] Faculty of Physics, Sofia University, Sofia, Bulgaria
[38] Faculty of Science, P.J. Šafárik University, Košice, Slovak Republic
[39] Frankfurt Institute for Advanced Studies, Johann Wolfgang Goethe-Universität Frankfurt, Frankfurt, Germany
[40] Fudan University, Shanghai, China
[41] Gangneung-Wonju National University, Gangneung, Republic of Korea
[42] Gauhati University, Department of Physics, Guwahati, India
[43] Helmholtz-Institut für Strahlen- und Kernphysik, Rheinische Friedrich-Wilhelms-Universität Bonn, Bonn, Germany
[44] Helsinki Institute of Physics (HIP), Helsinki, Finland
[45] High Energy Physics Group, Universidad Autónoma de Puebla, Puebla, Mexico
[46] Horia Hulubei National Institute of Physics and Nuclear Engineering, Bucharest, Romania
[47] Indian Institute of Technology Bombay (IIT), Mumbai, India
[48] Indian Institute of Technology Indore, Indore, India
[49] INFN, Laboratori Nazionali di Frascati, Frascati, Italy
[50] INFN, Sezione di Bari, Bari, Italy
[51] INFN, Sezione di Bologna, Bologna, Italy
[52] INFN, Sezione di Cagliari, Cagliari, Italy
[53] INFN, Sezione di Catania, Catania, Italy
[54] INFN, Sezione di Padova, Padova, Italy
[55] INFN, Sezione di Pavia, Pavia, Italy
[56] INFN, Sezione di Torino, Turin, Italy
[57] INFN, Sezione di Trieste, Trieste, Italy
[58] Inha University, Incheon, Republic of Korea
[59] Institute for Gravitational and Subatomic Physics (GRASP), Utrecht University/Nikhef, Utrecht, Netherlands
[60] Institute of Experimental Physics, Slovak Academy of Sciences, Košice, Slovak Republic
[61] Institute of Physics, Homi Bhabha National Institute, Bhubaneswar, India
[62] Institute of Physics of the Czech Academy of Sciences, Prague, Czech Republic
[63] Institute of Space Science (ISS), Bucharest, Romania
[64] Institut für Kernphysik, Johann Wolfgang Goethe-Universität Frankfurt, Frankfurt, Germany
[65] Instituto de Ciencias Nucleares, Universidad Nacional Autónoma de México, Mexico City, Mexico
[66] Instituto de Física, Universidade Federal do Rio Grande do Sul (UFRGS), Porto Alegre, Brazil
[67] Instituto de Física, Universidad Nacional Autónoma de México, Mexico City, Mexico
[68] iThemba LABS, National Research Foundation, Somerset West, South Africa
[69] Jeonbuk National University, Jeonju, Republic of Korea
[70] Johann-Wolfgang-Goethe Universität Frankfurt Institut für Informatik, Fachbereich Informatik und Mathematik, Frankfurt, Germany
[71] Korea Institute of Science and Technology Information, Daejeon, Republic of Korea
[72] KTO Karatay University, Konya, Turkey
[73] Laboratoire de Physique Subatomique et de Cosmologie, Université Grenoble-Alpes, CNRS-IN2P3, Grenoble, France
[74] Lawrence Berkeley National Laboratory, Berkeley, California, United States
[75] Lund University Department of Physics, Division of Particle Physics, Lund, Sweden
[76] Nagasaki Institute of Applied Science, Nagasaki, Japan
[77] Nara Women's University (NWU), Nara, Japan
[78] National and Kapodistrian University of Athens, School of Science, Department of Physics , Athens, Greece
[79] National Centre for Nuclear Research, Warsaw, Poland
[80] National Institute of Science Education and Research, Homi Bhabha National Institute, Jatni, India
[81] National Nuclear Research Center, Baku, Azerbaijan
[82] National Research and Innovation Agency - BRIN, Jakarta, Indonesia
[83] Niels Bohr Institute, University of Copenhagen, Copenhagen, Denmark
[84] Nikhef, National institute for subatomic physics, Amsterdam, Netherlands
[85] Nuclear Physics Group, STFC Daresbury Laboratory, Daresbury, United Kingdom
[86] Nuclear Physics Institute of the Czech Academy of Sciences, Husinec-Řež, Czech Republic
[87] Oak Ridge National Laboratory, Oak Ridge, Tennessee, United States

[88] Ohio State University, Columbus, Ohio, United States

[89] Physics department, Faculty of science, University of Zagreb, Zagreb, Croatia

[90] Physics Department, Panjab University, Chandigarh, India

[91] Physics Department, University of Jammu, Jammu, India

[92] Physics Program and International Institute for Sustainability with Knotted Chiral Meta Matter (SKCM2), Hiroshima University, Hiroshima, Japan

[93] Physikalisches Institut, Eberhard-Karls-Universität Tübingen, Tübingen, Germany

[94] Physikalisches Institut, Ruprecht-Karls-Universität Heidelberg, Heidelberg, Germany

[95] Physik Department, Technische Universität München, Munich, Germany

[96] Politecnico di Bari and Sezione INFN, Bari, Italy

[97] Research Division and ExtreMe Matter Institute EMMI, GSI Helmholtzzentrum für Schwerionenforschung GmbH, Darmstadt, Germany

[98] Saga University, Saga, Japan

[99] Saha Institute of Nuclear Physics, Homi Bhabha National Institute, Kolkata, India

[100] School of Physics and Astronomy, University of Birmingham, Birmingham, United Kingdom

[101] Sección Física, Departamento de Ciencias, Pontificia Universidad Católica del Perú, Lima, Peru

[102] Stefan Meyer Institut für Subatomare Physik (SMI), Vienna, Austria

[103] SUBATECH, IMT Atlantique, Nantes Université, CNRS-IN2P3, Nantes, France

[104] Sungkyunkwan University, Suwon City, Republic of Korea

[105] Suranaree University of Technology, Nakhon Ratchasima, Thailand

[106] Technical University of Košice, Košice, Slovak Republic

[107] The Henryk Niewodniczanski Institute of Nuclear Physics, Polish Academy of Sciences, Cracow, Poland

[108] The University of Texas at Austin, Austin, Texas, United States

[109] Universidad Autónoma de Sinaloa, Culiacán, Mexico

[110] Universidade de São Paulo (USP), São Paulo, Brazil

[111] Universidade Estadual de Campinas (UNICAMP), Campinas, Brazil

[112] Universidade Federal do ABC, Santo Andre, Brazil

[113] University of Cape Town, Cape Town, South Africa

[114] University of Derby, Derby, United Kingdom

[115] University of Houston, Houston, Texas, United States

[116] University of Jyväskylä, Jyväskylä, Finland

[117] University of Kansas, Lawrence, Kansas, United States

[118] University of Liverpool, Liverpool, United Kingdom

[119] University of Science and Technology of China, Hefei, China

[120] University of South-Eastern Norway, Kongsberg, Norway

[121] University of Tennessee, Knoxville, Tennessee, United States

[122] University of the Witwatersrand, Johannesburg, South Africa

[123] University of Tokyo, Tokyo, Japan

[124] University of Tsukuba, Tsukuba, Japan

[125] University Politehnica of Bucharest, Bucharest, Romania

[126] Universität Münster, Institut für Kernphysik, Münster, Germany

[127] Université Clermont Auvergne, CNRS/IN2P3, LPC, Clermont-Ferrand, France

[128] Université de Lyon, CNRS/IN2P3, Institut de Physique des 2 Infinis de Lyon, Lyon, France

[129] Université de Strasbourg, CNRS, IPHC UMR 7178, F-67000 Strasbourg, France, Strasbourg, France

[130] Université Paris-Saclay, Centre d'Etudes de Saclay (CEA), IRFU, Départment de Physique Nucléaire (DPhN), Saclay, France

[131] Université Paris-Saclay, CNRS/IN2P3, IJCLab, Orsay, France

[132] Università degli Studi di Foggia, Foggia, Italy

[133] Università del Piemonte Orientale, Vercelli, Italy

[134] Università di Brescia, Brescia, Italy

[135] Variable Energy Cyclotron Centre, Homi Bhabha National Institute, Kolkata, India

[136] Warsaw University of Technology, Warsaw, Poland

[137] Wayne State University, Detroit, Michigan, United States

[138] Wigner Research Centre for Physics, Budapest, Hungary

[139] Yale University, New Haven, Connecticut, United States

[140] Yonsei University, Seoul, Republic of Korea

[141] Zentrum für Technologie und Transfer (ZTT), Worms, Germany
[142] Affiliated with an institute covered by a cooperation agreement with CERN
[143] Affiliated with an international laboratory covered by a cooperation agreement with CERN.